A CONSENSUS-BASED DISTRIBUTED ALGORITHM FOR RECONFIGURATION OF SPACECRAFT FORMATIONS

by

Sonali Sinha Roy

A Thesis

Submitted to the Faculty of Purdue University

In Partial Fulfillment of the Requirements for the degree of

Master of Science in Aeronautics and Astronautics

School of Aeronautics and Astronautics

West Lafayette, Indiana

December 2020

THE PURDUE UNIVERSITY GRADUATE SCHOOL
STATEMENT OF COMMITTEE APPROVAL

Dr. Inseok Hwang, Co-chair

School of Aeronautics and Astronautics

Dr. Martin Corless, Co-chair

School of Aeronautics and Astronautics

Dr. Shaoshuai Mou

School of Aeronautics and Astronautics

Approved by:

Dr. Gregory Blaisdell

To my family, with love and gratitude

ACKNOWLEDGMENTS

I would like to express my sincerest gratitude to my advisors, Prof. Inseok Hwang and Prof. Martin Corless, for their constant support, encouragement, and advice. I would like to thank them for having faith in me and allowing me to take up this project. I have learnt a lot about the field not only in their respective classes but also through my research meetings with them. This work would not have been possible without their guidance and mentorship.

I am grateful to Prof. Shaoshuai Mou for introducing me to the concepts of multi-agent systems and control, which were instrumental in the completion of this project.

I would like to take this opportunity to thank Purdue University and the School of Aeronautics and Astronautics for all the facilities that have made education an enjoyable experience. I am thankful to all my professors at Purdue for their dedication to the advancement of Science.

I am also grateful to all the members of the Flight Dynamics & Control/Hybrid Systems Lab for their help and advice.

Lastly, I am deeply and eternally grateful to my family. Their love, care, and unwavering support has given me the courage to chase my dreams.

TABLE OF CONTENTS

LIST OF TABLES

LIST OF FIGURES

LIST OF SYMBOLS

ω	Angular velocity of orbit
μ	Gravitational parameter of central body
$\bar{r}$	Position vector
r	Radial distance
d_s	Separation distance
t	Time
I_n	Identity matrix of size $n \times n$
L_G	Laplacian of communication graph
X'	Conjugate transpose of matrix X
$X \otimes Y$	Kronecker product of matrix X with matrix Y

ABBREVIATIONS

CW	Clohessy-Wiltshire
LVLH	Local Vertical Local Horizontal
2BP	Two-Body Problem
BVP	Boundary Value Problem
TPBVP	Two-Point Boundary Value Problem
MIMO	Multi-input Multi-output
SRP	Solar Radiation Pressure
J_2	Second Zonal Harmonic Coefficient
RSS	Reconfigurable Space Structure
NASA	National Aeronautics and Space Administration (USA)
ESA	European Space Agency

ABSTRACT

Spacecraft formation flying refers to the coordinated operation of a group of spacecraft with a common objective. While the concept has been in existence for a long time, practical fruition of the ideas was not possible earlier due to technological limitations. The topic has received widespread attention in the last decade, with the development of autonomous control, improved computational facilities and better communication technology. It allows a number of small, lightweight, economical spacecraft to work together to execute the function of a larger, heavier, more complex and expensive spacecraft. The primary advantage of such systems is that they are flexible, modular, and cost-effective.

The flexibility of formation flying and other derived concepts comes from the fact that the units are not physically attached, allowing them to change position or orientation when the need arises. To fully realize this possibility, it is important to develop methods for spatial reorganization. This thesis is an attempt to contribute to this development.

In this thesis, the reconfiguration problem has been formulated as a single system with multiple inputs and multiple outputs, while preserving the individuality of the agents to a certain degree. The agents are able to communicate with their neighbors by sharing information. In this framework, a distributed closed-loop stabilizing controller has been developed, that would drive the spacecraft formation to a target shape. An expression for the controller gain as a function of the graph Laplacian eigenvalues has also been derived. The practical applications of this work have been demonstrated through simulations.

1. INTRODUCTION

Spacecraft (or satellite) formation flying is a concept of coordination among a group of spacecraft in order to accomplish a common goal. According to NASA Goddard Space Flight Center, it may be defined as "the tracking or maintenance of a desired relative separation, orientation, or position between or among spacecraft.[1]" It is a type of distributed space system.

The control tasks of satellite formation consist of relative orbit control and relative attitude control of satellites. The relative orbit control includes formation initialization, formation reconfiguration, and formation maintenance. Formation reconfiguration is different from the orbit transition of a single satellite, as it not only requires each satellite to complete the corresponding orbit transfer, but also requires coordinated movement of formation satellites. Formation initialization can be regarded as a typical formation reconfiguration. The relative positions of satellites in a formation are generally constrained in order to maintain the shape of the formation.

1.1 Background and Motivation

Spacecraft formation flying has become popular in recent times, with the development of autonomous flying and better communication technology. It allows a number of small, lightweight, economical spacecraft to work together to execute the function of a larger, heavier, more complex and expensive spacecraft. Such systems generally have a high accuracy, redundancy and dependability. They have traditionally been used for Earth observation, meteorology, communication, astronomy etc. However, there are plans by NASA and other space agencies to use this concept for deep space missions.

As technology advances and becomes more compact, the popularity of smaller satellites is rising. Small satellites are more cost effective and have rapid manufacturing times compared to larger spacecraft. While the functionality of the small satellites has risen over the years to rival that of larger satellites, some missions can't be accomplished with just one satellite. The solution is to assign multiple spacecraft to one mission.

The addition of multiple satellites to one mission also has led to added flexibility. Formation flying has allowed for more types of missions that wouldn't have been possible with just one satellite, even a larger one. For example, the Fourier Transform Spectrometer (FTS) CubeSat constellation of formation flying satellites will provide 3D observations of tropospheric winds [2].The inclusion of vertical atmospheric wind profiles will lead to improved and long-term weather forecasts. The possibility of replacing a faulty spacecraft at low cost or even reconfiguring the formation to exclude the dysfunctional satellite also increases mission flexibility. A formation can also be in a 'passive' orbit when not in use and can be deployed to an 'active' orbit via reorganization of its agents when the need arises.

Of course, manufacturing multiple satellites and putting them in orbit to accomplish a shared objective also comes with its own issues. All of the spacecraft must be able to communicate with one another and their geometry relative to one another must be maintained so that multiple spacecraft can accomplish the same goals as a large monolithic satellite.

The first discussion of flying multiple spacecraft for one mission was in 1977 [3]. The proposed mission was an infrared interferometer made up of multiple telescopes. It wasn't for another ten years after the genesis of this idea that another type of mission was proposed. This new type of mission considered using a two satellite architecture, a 'Leader' and a 'Follower' [4]. After this proposed mission, many studies were made concerning various architectures that could be utilized for these missions, and the interest in multiple spacecraft systems took off.

Scharf, Hadaegh, and Ploen [5] have arranged all satellite formations into six categories. The first is called Multiple-Input, Multiple-Output, where the controller treats the entire system as a multiple-input, multiple-output plant. With this type of architecture the familiar methods of modern control can be used, such as an LQR controller. The MIMO approach has been used by Schaub and Alfriend [6] for controlling a formation of geometrically identical satellites. A Leader/Follower architecture involves a "Leader" satellite which is tracked by all of the "Follower" satellites. This type of formation is the most popular, because it reduces an entire formation control into a simpler set of tracking problems. This has been extensively worked on by Mesbahi and Hadaegh [7], Wang and Hadaegh [8], and Schlanbusch [9]. If the spacecraft in the formation are treated as rigid bodies inside of a virtual rigid structure, they are in what is known as a Virtual Structure. The motion of the large, virtual structure and the constant position of each of the spacecraft are used to track individual spacecraft. Cyclic formations are similar to Leader/Follower architectures, except that there is not one lead satellite. Instead the interconnection between the satellites lead to cyclic dependencies. Zhang and Gurfil [10] have developed a cyclic control law for long time scales utilizing fixed-magnitude thrusters. The last type of formation flying is the Behavioral architecture which is composed of satellites with controllers that are designed to achieve different behaviors. It has been used by McInnes [11] to maintain an annular formation in orbit.

As mentioned earlier, the rise in popularity of formation flying has grown in the last twenty-five years. As a result, more than thirty formation flying satellite missions have been launched since 2000, with at least six new missions planned in the next five years [12]. But these missions are not only restricted to individual, independent satellites flying in formation. The more recent proposals include concepts like adaptive or reconfigurable space structures and fractionated telescopes among others.

The motivation for reconfigurable space structures arises from the investment and complexity involved in designing, assembling, and maintaining large space structures such as the International Space Station. The ISS has 16 modules and is made of hundreds of parts, some of which are shown in Fig. (1.1). Any malfunction in one part invokes a tedious replacement process that may take days to complete, sometimes at a high financial costs. Reconfigurable structures have been proposed for easy and low-cost maintenance or replacement in case of damage, along with the added benefit of situational adaptability.

Similarly, the cost and complexity of on-orbit assembly of telescopes like Hubble have served as the motivation for the development of fractionated telescopes and interferometers.

For the full functionality of formations and fragmented space architecture, it is necessary to develop robust methods of spatial reorientation of these spacecraft clusters. This need has inspired the work conducted in this thesis.

1.2 Objectives and Organization

The goal of this thesis is to demonstrate methods of shape reconfiguration of spacecraft formations and illustrate their potential applications. The development of a distributed

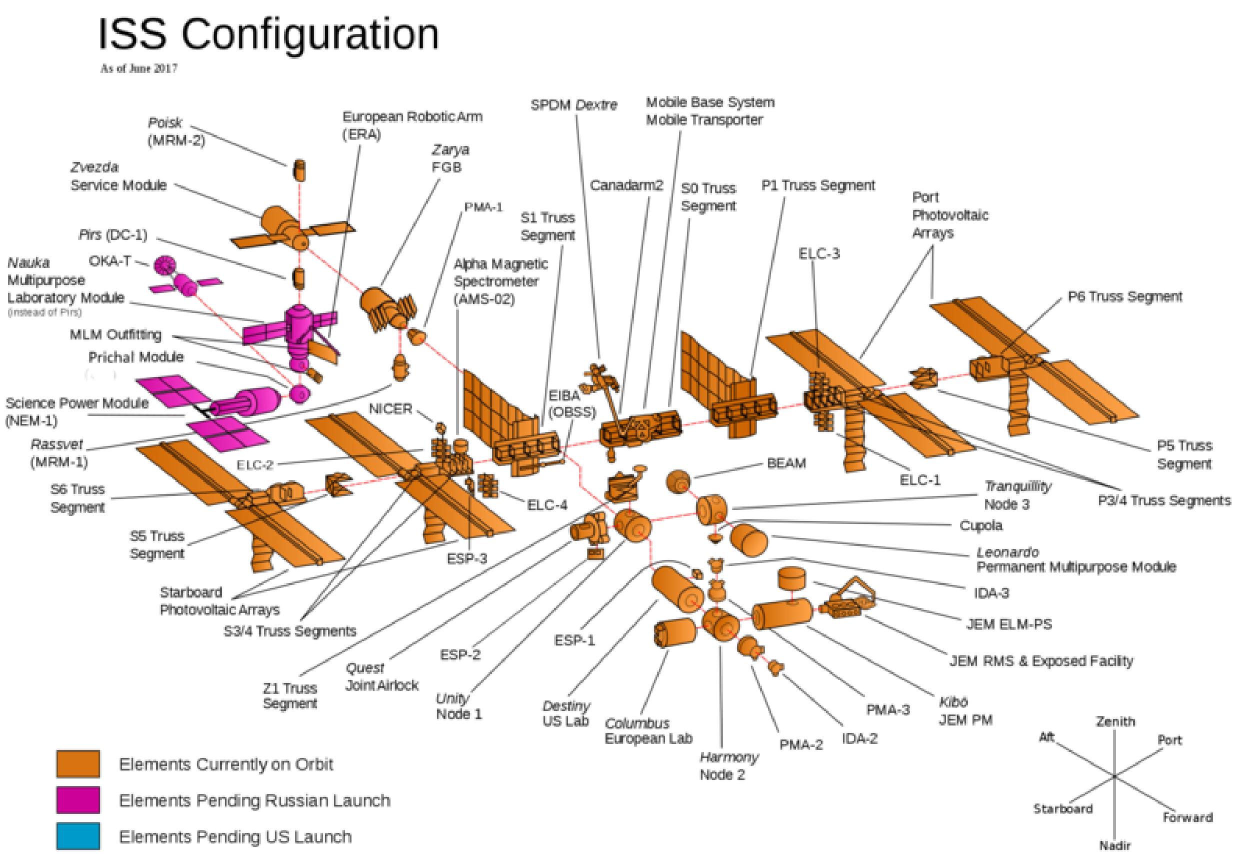

Figure 1.1. Construction of the ISS [13]

stabilizing feedback controller was attempted and an expression for selecting the same has been derived in this thesis. The model has been validated through numerical simulations.

The organization of this thesis is as follows. In Chapter 2, the equations of motion have been derived and then linearized. The frames of reference used throughout the work have been described here. In Chapter 3, the reconfiguration problem has been formulated as a two-point boundary value problem. Chapter 4 contains the closed loop formulation. The main result of this thesis has been derived in Chapter 4, Section 4.4. In Chapter 5, applications of this work have been shown and some concluding remarks have been provided in Chapter 6.

2. PROBLEM DESCRIPTION

The problem dealt with in this thesis is essentially the repositioning of a set of spacecraft agents such that the resulting formation is in the targeted final shape. The following assumptions have been made:

- The formation is in the vicinity of a large celestial body (Earth, Moon, Sun etc.).
- Each individual agent is small in mass in comparison to the above-mentioned celestial body and therefore, they are considered to be as point masses.
- The motion of the agents is primarily affected by the gravitational force exerted by the celestial body, and all other natural perturbing forces are very small.

Essentially, these assumptions signify that the problem may be treated as a "two-body problem (2BP)", with the formation being in orbit around the celestial body or the central body. For any point mass at a distance r from the center of the celestial body, the equation of motion is derived from Newton's Second Law and the Law of Gravitation as:

$$\frac{{}^{\mathrm{i}}d^2\bar{r}}{dt^2} = -\mu\frac{\bar{r}}{r^3} \tag{2.1}$$

Here, $\bar{r}$ is the position vector with respect to an inertial frame of reference with the origin at the center of the central body. μ is called the gravitational parameter of the central body, and is equal to the universal gravitational constant G times the mass m of the central body, i.e., $\mu = Gm$.

As all the agents in the formation are close to each other and are orbiting the same central body, it is convenient to define the equations of motion with respect to a rotating frame of reference.

2.1 Equations of Motion in the LVLH Frame

The *Local Vertical, Local Horizontal Frame* or *LVLH Frame* is a rotating frame that moves with a reference point which is in a circular orbit around the central body. In this reference frame, the origin is at the center of the central body, x is in the radial direction

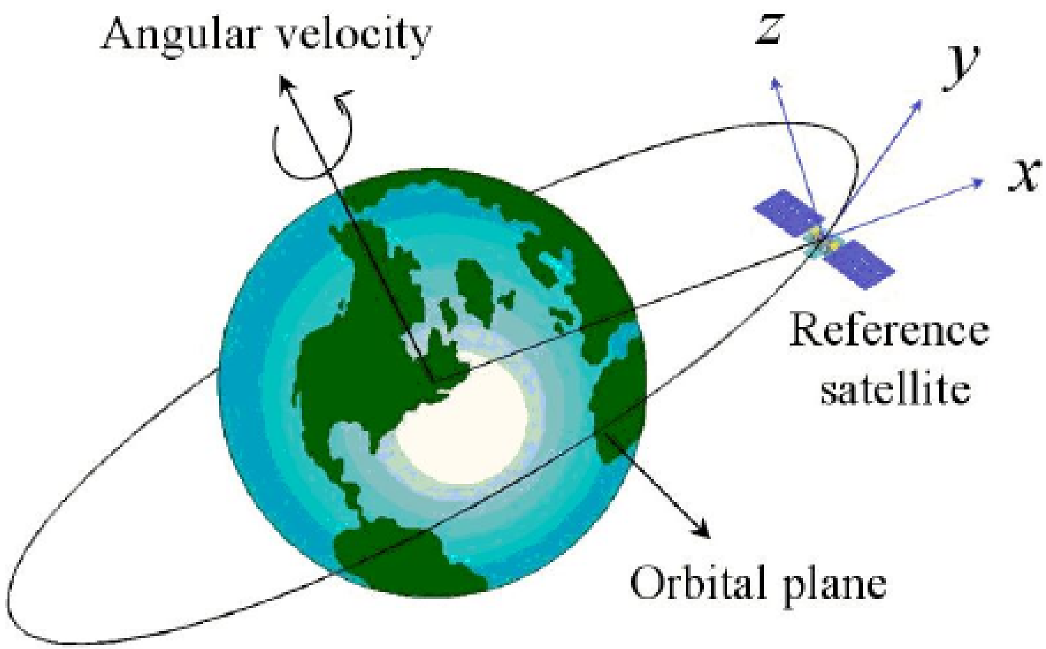

Figure 2.1. Geocentric LVLH Frame [14]

pointing away from the central body, y points in the direction of velocity, and z completes the right-handed coordinate system. Therefore, motion along x, y and z axis is considered 'radial', 'along-track', and 'out-of-plane' respectively. This is shown for a geocentric LVLH frame in Fig. (2.1)

For this problem, it is considered that the reference point is moving along a circular orbit around the central body a constant angular velocity $\bar{\omega}$. The angular velocity is, therefore, $\bar{\omega} = \omega\hat{z}$, where ω is a constant. The velocity of a point mass at $\bar{r} = x\hat{x} + y\hat{y} + z\hat{z}$ (in LVLH coordinates) can be derived using the Basic Kinematic Equation (BKE).

$$\frac{{}^{\mathrm{i}}d\bar{r}}{dt} = \frac{{}^{l}d\bar{r}}{dt} + \bar{\omega} \times \bar{r} \tag{2.2}$$

Here the prescripts i and l represent the inertial and rotating (LVLH) frame respectively. The equation of motion in the LVLH frame can be derived using the BKE again.

$$
\begin{aligned}
\frac{{}^{\mathrm{i}}d^2\bar{r}}{dt^2} &= \frac{{}^{\mathrm{i}}d}{dt}\left[\frac{{}^{l}d\bar{r}}{dt} + \bar{\omega}\times\bar{r}\right] \\
&= \frac{{}^{l}d}{dt}\left[\frac{{}^{l}d\bar{r}}{dt} + \bar{\omega}\times\bar{r}\right] + \bar{\omega}\times\left[\frac{{}^{l}d\bar{r}}{dt} + \bar{\omega}\times\bar{r}\right] \\
&= \frac{{}^{l}d^2\bar{r}}{dt^2} + \cancelto{0}{\frac{{}^{l}d\bar{\omega}}{dt}}\times\bar{r} + 2\bar{\omega}\times\frac{{}^{l}d\bar{r}}{dt} + \bar{\omega}\times(\bar{\omega}\times\bar{r}) \\
&= \frac{{}^{l}d^2\bar{r}}{dt^2} + 2\bar{\omega}\times\frac{{}^{l}d\bar{r}}{dt} + (\bar{\omega}\cdot\bar{r})\bar{\omega} - (\bar{\omega}\cdot\bar{\omega})\bar{r}
\end{aligned}
$$

Using equation (2.1),

$$
\begin{aligned}
-\mu\frac{\bar{r}}{r^3} &= \frac{{}^{l}d^2\bar{r}}{dt^2} + 2\bar{\omega}\times\frac{{}^{l}d\bar{r}}{dt} + (\bar{\omega}\cdot\bar{r})\bar{\omega} - \omega^2\bar{r} \\
\implies -\mu\frac{\bar{r}}{r^3} &= \ddot{\bar{r}} + 2\bar{\omega}\times\dot{\bar{r}} + (\bar{\omega}\cdot\bar{r})\bar{\omega} - \omega^2\bar{r} \qquad (2.3)
\end{aligned}
$$

The left-hand side of equation (2.3) is

$$
\text{LHS} = -\frac{\mu}{r^3}(x\,\hat{x} + y\,\hat{y} + z\,\hat{z}) \qquad (2.4)
$$

where, $r = \sqrt{x^2 + y^2 + z^2}$. The right-hand side is

$$
\begin{aligned}
\text{RHS} &= (\ddot{x}\hat{x} + \ddot{y}\hat{y} + \ddot{z}\hat{z}) + 2(\omega\hat{z})\times(\dot{x}\hat{x} + \dot{y}\hat{y} + \dot{z}\hat{z}) + (\omega\hat{z})\cdot(x\hat{x} + y\hat{y} + z\hat{z})(\omega\hat{z}) \\
&\quad - \omega^2(x\hat{x} + y\hat{y} + z\hat{z}) \\
&= (\ddot{x}\hat{x} + \ddot{y}\hat{y} + \ddot{z}\hat{z}) + 2\omega(\dot{x}\hat{y} - \dot{y}\hat{x}) + \omega^2 zhatz - \omega^2(x\hat{x} + y\hat{y} + z\hat{z}) \\
&= (\ddot{x}\hat{x} + \ddot{y}\hat{y} + \ddot{z}\hat{z}) + 2\omega(\dot{x}\hat{y} - \dot{y}\hat{x}) - \omega^2 x\hat{x} - \omega^2 y\hat{y} \\
\implies \text{RHS} &= (\ddot{x} - 2\omega\dot{y} - \omega^2 x)\,\hat{x} + (\ddot{y} + 2\omega\dot{x} - \omega^2 y)\,\hat{y} + \ddot{z}\,\hat{z} \qquad (2.5)
\end{aligned}
$$

Equating the x, y, z components of LHS to those of RHS gives the following set of equations, which form the equations of motion in each direction in the LVLH frame.

$$\ddot{x} = 2\omega\dot{y} + (\omega^2 - \frac{\mu}{r^3})x \tag{2.6a}$$

$$\ddot{y} = -2\omega\dot{x} + (\omega^2 - \frac{\mu}{r^3})y \tag{2.6b}$$

$$\ddot{z} = -\frac{\mu}{r^3}z \tag{2.6c}$$

In the presence of an applied acceleration (i.e., control input) u_x, u_y, u_z in the x, y, z direction respectively, equation (2.6) becomes

$$\ddot{x} = 2\omega\dot{y} + (\omega^2 - \frac{\mu}{r^3})x + u_x \tag{2.7a}$$

$$\ddot{y} = -2\omega\dot{x} + (\omega^2 - \frac{\mu}{r^3})y + u_y \tag{2.7b}$$

$$\ddot{z} = -\frac{\mu}{r^3}z + u_z \tag{2.7c}$$

These are the nonlinear equations of motion for a spacecraft in the x, y and z directions in the LVLH frame.

2.2 Clohessy-Wiltshire Equations

The Clohessy-Wiltshire equations were derived in 1960 by W.H. Clohessy and R.S. Wiltshire [15]. These equations were formulated as the linear approximation of the nonlinear orbit dynamics for the satellite rendezvous problem, considering each spacecraft as a point mass. They represent the linearized relative motion of a 'chaser' with respect to a target spacecraft in a circular orbit about a central body. Over time, they have evolved as the standard set of equations for defining the dynamics of spacecraft formations.

2.2.1 Equilibrium Position

To represent the dynamics of the formation in terms of the Clohessy-Wiltshire equations, the equations of motion must be linearized about an equilibrium point. Let $\bar{r}_{\mathrm{e}}$ be an equilibrium position. Therefore, $\dot{\bar{r}}_{\mathrm{e}} = 0$ and $\ddot{\bar{r}}_{\mathrm{e}} = 0$. Substituting these values in equation (2.3) results in

$$-\mu \frac{\bar{r}_{\mathrm{e}}}{{r_{\mathrm{e}}}^3} = (\bar{\omega} \cdot \bar{r}_{\mathrm{e}})\bar{\omega} - \omega^2 \bar{r}_{\mathrm{e}} \tag{2.8}$$

Taking the dot product with $\bar{\omega}$ yields

$$\begin{aligned} -\mu \frac{\bar{\omega} \cdot \bar{r}_{\mathrm{e}}}{{r_{\mathrm{e}}}^3} &= (\bar{\omega} \cdot \bar{r}_{\mathrm{e}})(\bar{\omega} \cdot \bar{\omega}) - \omega^2 (\bar{\omega} \cdot \bar{r}_{\mathrm{e}}) \\ &= \omega^2 (\bar{\omega} \cdot \bar{r}_{\mathrm{e}}) - \omega^2 (\bar{\omega} \cdot \bar{r}_{\mathrm{e}}) \\ \implies -\mu \frac{\bar{\omega} \cdot \bar{r}_{\mathrm{e}}}{{r_{\mathrm{e}}}^3} &= 0 \end{aligned} \tag{2.9}$$

Since $\frac{\mu}{{r_{\mathrm{e}}}^3} \neq 0$, hence $\bar{\omega} \cdot \bar{r}_{\mathrm{e}} = 0$. From equation (2.8),

$$-\mu \frac{\bar{r}_{\mathrm{e}}}{{r_{\mathrm{e}}}^3} = -\omega^2 \bar{r}_{\mathrm{e}} \tag{2.10}$$

$$\begin{aligned} \implies \frac{\mu}{{r_{\mathrm{e}}}^3} &= \omega^2 \\ \implies r_{\mathrm{e}} &= \left(\frac{\mu}{\omega^2}\right)^{1/3} \end{aligned} \tag{2.11}$$

An equilibrium position $\bar{r}_{\mathrm{e}} = r_{\mathrm{e}}\,\hat{x}$ is selected, placing it on the reference orbit used to define the current LVLH frame.

2.2.2 Linearization about the Equilibrium

The LVLH equation of motion i.e., equation (2.3) is linearized about the equilibrium solution $\bar{r}_{\mathrm{e}}$. Let $\delta\bar{r} = \bar{r} - \bar{r}_{\mathrm{e}}$.

$$
\begin{aligned}
-\frac{\mu}{{r_\mathrm{e}}^3}\delta\bar{r} + 3\frac{\mu}{{r_\mathrm{e}}^4}\delta\bar{r}\,\bar{r}_\mathrm{e} &= \delta\ddot{\bar{r}} + 2\bar{\omega}\times\delta\dot{\bar{r}} + (\bar{\omega}\cdot\delta\bar{r})\bar{\omega} - \omega^2\delta\bar{r} \\
\implies -\omega^2\delta\bar{r} + 3\frac{\omega^2}{r_\mathrm{e}}\delta r\,\bar{r}_\mathrm{e} &= \delta\ddot{\bar{r}} + 2\bar{\omega}\times\delta\dot{\bar{r}} + (\bar{\omega}\cdot\delta\bar{r})\bar{\omega} - \omega^2\delta\bar{r} \\
\implies 3\frac{\omega^2}{r_\mathrm{e}}\delta r\,\bar{r}_\mathrm{e} &= \delta\ddot{\bar{r}} + 2\bar{\omega}\times\delta\dot{\bar{r}} + (\bar{\omega}\cdot\delta\bar{r})\bar{\omega} \qquad (2.12)
\end{aligned}
$$

It is to be noted that the variables are defined as follows:

$$\bar{r}_\mathrm{e} = r_\mathrm{e}\,\hat{x} \qquad (2.13)$$

$$\bar{\omega} = \omega\,\hat{z} \qquad (2.14)$$

$$\bar{r} = x\,\hat{x} + y\,\hat{y} + z\,\hat{z} \qquad (2.15)$$

$$\delta\bar{r} = \delta x\,\hat{x} + \delta y\,\hat{y} + \delta z\,\hat{z} = (x - r_\mathrm{e})\,\hat{x} + y\,\hat{y} + z\,\hat{z} \qquad (2.16)$$

Then,

$$r^2 = x^2 + y^2 + z^2 \qquad (2.17)$$

Using linear approximation,

$$
\begin{aligned}
2r_\mathrm{e}\delta r &\approx 2x_\mathrm{e}\delta x + 2y_\mathrm{e}\delta y + 2z_\mathrm{e}\delta z \\
\implies 2r_\mathrm{e}\delta r &\approx 2r_\mathrm{e}\delta x \\
\implies \delta r &\approx \delta x \qquad (2.18)
\end{aligned}
$$

Additionally,

$$\bar{\omega} \times \delta\dot{\bar{r}} = (\omega\,\hat{z}) \times (\delta\dot{x}\,\hat{x} + \delta\dot{y}\,\hat{y} + \delta\dot{z}\,\hat{z}) \\ = \omega(\delta\dot{x}\,\hat{y} - \delta\dot{y}\,\hat{x}) \tag{2.19}$$

$$\bar{\omega} \cdot \delta\bar{r} = (\omega\,\hat{z}) \cdot (\delta x\,\hat{x} + \delta y\,\hat{y} + \delta z\,\hat{z}) \\ = \omega\delta z \tag{2.20}$$

Substituting these values in equation (2.12) yields

$$3\frac{\omega^2}{r_e}\delta x\, r_e\,\hat{x} = (\delta\ddot{x}\,\hat{x} + \delta\ddot{y}\,\hat{y} + \delta\ddot{z}\,\hat{z}) + 2\omega(\delta\dot{x}\,\hat{y} - \delta\dot{y}\,\hat{x}) + \omega^2\delta z\hat{z} \\ \Longrightarrow (\delta\ddot{x} - 2\omega\delta\dot{y} - 3\omega^2\delta x)\hat{x} + (\delta\ddot{y} + 2\omega\delta\dot{x})\hat{y} + (\delta\ddot{z} + \omega^2\delta z)\hat{z} = 0 \tag{2.21}$$

Separating the x, y, z components results in the famous Clohessy-Wiltshire equations of motion.

$$\delta\ddot{x} - 2\omega\delta\dot{y} - 3\omega^2\delta x = 0 \tag{2.22a}$$

$$\delta\ddot{y} + 2\omega\delta\dot{x} = 0 \tag{2.22b}$$

$$\delta\ddot{z} + \omega^2\delta z = 0 \tag{2.22c}$$

When control inputs u_x, u_y, u_z are applied in the x, y, z directions respectively, the new linearized equations of motion are

$$\delta\ddot{x} = 2\omega\delta\dot{y} + 3\omega^2\delta x + u_x \tag{2.23a}$$

$$\delta\ddot{y} = -2\omega\delta\dot{x} + u_y \tag{2.23b}$$

$$\delta\ddot{z} = -\omega^2\delta z + u_z \tag{2.23c}$$

A spacecraft's motion is defined completely using six states. If the three components of motion and velocity are selected as these states then the state vector $\delta\mathbf{x}$ is

$$\delta\mathbf{x} = \begin{bmatrix} \delta x \\ \delta y \\ \delta z \\ \delta\dot{x} \\ \delta\dot{y} \\ \delta\dot{z} \end{bmatrix} \tag{2.24}$$

The input vector $\delta\mathbf{u}$ is

$$\delta\mathbf{u} = \begin{bmatrix} u_x \\ u_y \\ u_z \end{bmatrix} \tag{2.25}$$

The dynamics of the spacecraft can now be represented as a linear system.

$$\delta\dot{\mathbf{x}} = A\delta\mathbf{x} + B\delta\mathbf{u} \tag{2.26}$$

where,

$$A = \begin{bmatrix} 0 & 0 & 0 & 1 & 0 & 0 \\ 0 & 0 & 0 & 0 & 1 & 0 \\ 0 & 0 & 0 & 0 & 0 & 1 \\ 3\omega^2 & 0 & 0 & 0 & 2\omega & 0 \\ 0 & 0 & 0 & -2\omega & 0 & 0 \\ 0 & 0 & -\omega^2 & 0 & 0 & 0 \end{bmatrix} \tag{2.27}$$

and,

$$B = \begin{bmatrix} 0 & 0 & 0 \\ 0 & 0 & 0 \\ 0 & 0 & 0 \\ 1 & 0 & 0 \\ 0 & 1 & 0 \\ 0 & 0 & 1 \end{bmatrix} \tag{2.28}$$

Here, ω is the constant angular velocity of the reference orbit.

Henceforth, throughout this thesis, A and B shall denote the above-mentioned matrices unless specified otherwise.

2.3 Use of CW Dynamics in the Thesis

The goal of this work is to demonstrate the shape reconfiguration of a spacecraft formation. It is assumed that a set of spacecraft agents are initially in a formation of one shape and these agents must change their positions to form a new shape. In the chapters that follow, this reconfiguration problem shall be formulated in two different ways, both based on the CW linearized dynamics derived here.

In Chapter 3, the reconfiguration problem has been formulated as a two-point boundary value problem. This requires complete knowledge of the initial and final states (i.e., both position and velocity) of each agent in the formation. These are used as boundary conditions and each agent is driven to follow a trajectory from its own initial state to final state such that the overall fuel consumption of the whole formation is minimized. This method is non-ideal for several reasons, which have been discussed at the end of the chapter. The two major drawbacks are that this is an open-loop control, and it requires the exact final state to be specified.

In Chapter 4, an alternative formulation is presented, with a goal of eliminating some of the shortcomings of the TPBVP formulation from Chapter 3. This formulation involves a closed-loop control and assumes that the agents share information through a network specified by the communication graph. The need to know the exact final state of each agent is eliminated by introducing a reference target configuration, represented by the vector h, and by incorporating consensus theory into the formulation. In this case, only the relative positions of the agents in the target shape need to be known. The final configuration is in the same shape as described by the vector h, but the positions for all the agents are offset by a constant vector p, which may or may not be zero. Through communication among agents, the formation converges to the shape specified by h and reaches consensus on the offset p and the common velocity.

It is to be noted that throughout this thesis, the word 'state' refers to the exact values of position and velocity coordinates in a given reference frame, while 'shape' refers to the geometric form created by the spatial positions of the agents. Therefore, when a formation converges to a specified shape, it means that the relative distances and orientations of the agents are the same as those of the vertices of this particular shape. The actual position coordinates of the agents do not necessarily coincide with the vertices of the given shape.

3. TWO-POINT BOUNDARY VALUE PROBLEM FORMULATION

The shape reconfiguration of the formation may be treated as a boundary value problem that solves the Clohessy-Wiltshire equations while also satisfying the boundary conditions, i.e., the initial state and the final state of the formation. Using the calculus of variations approach, this can be formulated as an optimal control problem, which can be solved numerically.

The Clohessy-Wiltshire equations define the linearized dynamics of each agent in the formation. The initial and targeted final configuration of the formation are used as the boundary conditions. A cost function may be selected based on the goal of the problem. Using the variational approach, the necessary conditions for optimality may be obtained.

Let n be the number of agents in the formation. Let $\tilde{\mathbf{x}}$ and $\tilde{\mathbf{u}}$ be the concatenated state and input vectors, that contain the states of inputs for all the agents. Therefore,

$$\tilde{\mathbf{x}} = \begin{bmatrix} \delta\mathbf{x}_1 \\ \delta\mathbf{x}_2 \\ \vdots \\ \delta\mathbf{x}_n \end{bmatrix} \quad \text{and} \quad \tilde{\mathbf{u}} = \begin{bmatrix} \delta\mathbf{u}_1 \\ \delta\mathbf{u}_2 \\ \vdots \\ \delta\mathbf{u}_n \end{bmatrix} \tag{3.1}$$

Here $\delta\mathbf{x}_\mathrm{i}$ is the linearized state vector and $\delta\mathbf{u}_\mathrm{i}$ is the input vector for the i^{th} agent.

It is assumed that the initial position and target position of each agent are determined and known beforehand, i.e., each agent is chasing a fixed target. It is also assumed that the target must be achieved within a specified time, making this a fixed time problem.

3.1 Cost Function, Boundary Conditions, Dynamics, and Constraint

To demonstrate the reconfiguration procedure, the cost function is selected for fuel optimization. At any instant, the fuel consumption of a spacecraft is directly proportional to the applied acceleration i.e., control input. Thus, the cost J to be optimized is

$$J = \frac{1}{2}\int_0^{t_f} \tilde{\mathbf{u}}(t)^T \tilde{\mathbf{u}}(t)\, dt \tag{3.2}$$

Let the initial configuration of the formation be defined by the vector $\tilde{\mathbf{x}}_0$ and the final configuration by $\tilde{\mathbf{x}}_f$. These vectors contain the position and velocity of each agent in the formation. Therefore the boundary conditions are represented as

$$\tilde{\mathbf{x}}(0) = \tilde{\mathbf{x}}_0 \tag{3.3a}$$

$$\tilde{\mathbf{x}}(t_f) = \tilde{\mathbf{x}}_f \tag{3.3b}$$

The states for a single agent, i, have been defined as,

$$\delta\mathbf{x}_{\mathrm{i}} = \begin{pmatrix} \delta x \\ \delta y \\ \delta z \\ \delta\dot{x} \\ \delta\dot{y} \\ \delta\dot{z} \end{pmatrix} \tag{3.4}$$

Using the Clohessy-Wiltshire equations, the dynamics of each agent can be defined as

$$\delta\dot{\mathbf{x}}_\mathrm{i} = \underbrace{\begin{bmatrix} 0 & 0 & 0 & 1 & 0 & 0 \\ 0 & 0 & 0 & 0 & 1 & 0 \\ 0 & 0 & 0 & 0 & 0 & 1 \\ 3\omega^2 & 0 & 0 & 0 & 2\omega & 0 \\ 0 & 0 & 0 & -2\omega & 0 & 0 \\ 0 & 0 & -\omega^2 & 0 & 0 & 0 \end{bmatrix}}_{A} \delta\mathbf{x}_\mathrm{i} + \underbrace{\begin{bmatrix} 0 & 0 & 0 \\ 0 & 0 & 0 \\ 0 & 0 & 0 \\ 1 & 0 & 0 \\ 0 & 1 & 0 \\ 0 & 0 & 1 \end{bmatrix}}_{B} \delta\mathbf{u}_\mathrm{i} \tag{3.5}$$

Therefore, the dynamics of the whole formation can be defines as

$$\dot{\tilde{\mathbf{x}}} = \begin{bmatrix} A & 0 & \dots & 0 \\ 0 & A & \dots & 0 \\ \vdots & \vdots & \ddots & \vdots \\ 0 & 0 & \dots & A \end{bmatrix} \tilde{\mathbf{x}} + \begin{bmatrix} B & 0 & \dots & 0 \\ 0 & B & \dots & 0 \\ \vdots & \vdots & \ddots & \vdots \\ 0 & 0 & \dots & B \end{bmatrix} \tilde{\mathbf{u}} \tag{3.6}$$

$$\implies \dot{\tilde{\mathbf{x}}} = A_f \tilde{\mathbf{x}} + B_f \tilde{\mathbf{u}} \tag{3.7}$$

where,

$$A_f = I_n \otimes A$$
$$B_f = I_n \otimes B$$

Here, $\otimes$ denotes the Kronecker product.

In most realistic scenarios, the control input to the spacecraft is limited by the capabilities of the engine or thruster. Therefore, it is sensible to impose bounds on the magnitude of input in each direction for all agents. For the i^{th} element u_i of the concatenated input vector $\tilde{\mathbf{u}}$, this can be represented as:

$$|u_\mathrm{i}| \leq U \tag{3.8}$$

3.2 Unconstrained Two-Point Boundary Value Problem

The optimal control problem, without the constraints, may be formulated by introducing the co-state (or Lagrange multiplier), λ and defining the Hamiltonian as:

$$\mathcal{H} = \frac{\partial J}{\partial t} + \boldsymbol{\lambda}^T \dot{\tilde{\mathbf{x}}} \tag{3.9}$$

$$\implies \mathcal{H} = \frac{1}{2}(\tilde{\mathbf{u}}^T \tilde{\mathbf{u}}) + \boldsymbol{\lambda}^T (A_f \tilde{\mathbf{x}} + B_f \tilde{\mathbf{u}}) \tag{3.10}$$

The dynamics of the co-states is given by

$$\dot{\boldsymbol{\lambda}} = -\left(\frac{\partial \mathcal{H}}{\partial \tilde{\mathbf{x}}}\right)^T \tag{3.11}$$

$$= -\left[\frac{\partial}{\partial \tilde{\mathbf{x}}}(\boldsymbol{\lambda}^T A_f \tilde{\mathbf{x}})\right]^T$$

$$\dot{\boldsymbol{\lambda}} = -A_f^T \boldsymbol{\lambda} \tag{3.12}$$

The optimal control can be obtained by using the necessary condition

$$\frac{\partial \mathcal{H}}{\partial \tilde{\mathbf{u}}} = 0 \tag{3.13}$$

$$\implies \frac{\partial}{\partial \tilde{\mathbf{u}}}\left(\frac{1}{2}\tilde{\mathbf{u}}^T \tilde{\mathbf{u}} + \boldsymbol{\lambda}^T B_f \tilde{\mathbf{u}}\right) = 0$$

$$\implies \frac{2\tilde{\mathbf{u}}^T}{2} + \boldsymbol{\lambda}^T B_f = 0$$

$$\implies \tilde{\mathbf{u}} = -B_f^T \boldsymbol{\lambda} \tag{3.14}$$

Therefore, the fuel-optimal reconfiguration of the formation can be represented as a Two Point Boundary Value Problem using the state and co-state equations (3.7, 3.12), optimal control equation (3.14) and boundary conditions (3.3). This is summarized in Table 3.1.

Table 3.1. Two-Point Boundary Value Problem (TPBVP)

Variable	**Dynamics**	**Initial**	**Final**
$\tilde{\mathbf{x}}$	$\dot{\tilde{\mathbf{x}}} = A_f \tilde{\mathbf{x}} - B_f B_f^T \boldsymbol{\lambda}$	$\tilde{\mathbf{x}}(0) = \tilde{\mathbf{x}}_0$	$\tilde{\mathbf{x}}(t_f) = \tilde{\mathbf{x}}_f$
$\boldsymbol{\lambda}$	$\dot{\boldsymbol{\lambda}} = -A_f^T \boldsymbol{\lambda}$	N/A	N/A

3.3 Constrained Two-Point Boundary Value Problem Formulation

When the control bounds are imposed, the optimal control equation is replaced by Pontryagin's Minimum Principle,

$$\mathcal{H}(\tilde{\mathbf{x}}^*, \tilde{\mathbf{u}}^*, \boldsymbol{\lambda}^*, t) \le \mathcal{H}(\tilde{\mathbf{x}}^*, \tilde{\mathbf{u}}, \boldsymbol{\lambda}^*, t) \quad \text{when } |u_{\rm i}| \le U \tag{3.15}$$

$$\implies \frac{1}{2}(\tilde{\mathbf{u}}^{*T}\tilde{\mathbf{u}}^*) + \boldsymbol{\lambda}^T(A_f\tilde{\mathbf{x}} + B_f\tilde{\mathbf{u}}^*) \le \frac{1}{2}(\tilde{\mathbf{u}}^T\tilde{\mathbf{u}}) + \boldsymbol{\lambda}^T(A_f\tilde{\mathbf{x}} + B_f\tilde{\mathbf{u}})$$

$$\implies \frac{1}{2}\sum_{\rm i=1}^{3n} u_{\rm i}^{*2} + \boldsymbol{\lambda}^T B_f \tilde{\mathbf{u}}^* \le \frac{1}{2}\sum_{\rm i=1}^{3n} u_{\rm i}^{2} + \boldsymbol{\lambda}^T B_f \tilde{\mathbf{u}} \tag{3.16}$$

Let $b_{\rm i}$ be the $\rm i^{th}$ column of B_f. Therefore, the above equation may be represented in terms of each individual $u_{\rm i}$ as

$$\frac{1}{2}u_{\rm i}^{*2} + \boldsymbol{\lambda}^T b_{\rm i} u_{\rm i}^* \le \frac{1}{2}u_{\rm i}^{2} + \boldsymbol{\lambda}^T b_{\rm i} u_{\rm i}^* \tag{3.17}$$

$$\implies \frac{1}{2}\left[\left(u_{\rm i}^* + \boldsymbol{\lambda}^T b_{\rm i}\right)^2 - \left(\boldsymbol{\lambda}^T b_{\rm i}\right)^2\right] \le \frac{1}{2}\left[\left(u_{\rm i} + \boldsymbol{\lambda}^T b_{\rm i}\right)^2 - \left(\boldsymbol{\lambda}^T b_{\rm i}\right)^2\right]$$

$$\implies \left(u_{\rm i}^* + \boldsymbol{\lambda}^T b_{\rm i}\right)^2 \le \left(u_{\rm i} + \boldsymbol{\lambda}^T b_{\rm i}\right)^2 \tag{3.18}$$

Case I: $\boldsymbol{\lambda}^T b_{\rm i} < -U$ The minimum value of the right-hand side is attained at $u_{\rm i} = U$.

Case II: $\boldsymbol{\lambda}^T b_{\rm i} > U$ The minimum value of the right-hand side is attained at $u_{\rm i} = -U$.

Case III: $-U \leq \boldsymbol{\lambda}^T b_{\mathrm{i}} \leq U$ The minimum value of the right-hand side is attained at $u_{\mathrm{i}} = -\boldsymbol{\lambda}^T b_{\mathrm{i}}$.

Therefore, the optimal control for the $\mathrm{i}^t h$ agent is given by

$$u_{\mathrm{i}}^* = \begin{cases} -U & \text{if } \boldsymbol{\lambda}^T b_{\mathrm{i}} > U \\ -\boldsymbol{\lambda}^T b_{\mathrm{i}} & \text{if } -U \leq \boldsymbol{\lambda}^T b_{\mathrm{i}} \leq U \\ +U & \text{if } \boldsymbol{\lambda}^T b_{\mathrm{i}} < -U \end{cases} \quad \forall u_{\mathrm{i}} \in \tilde{\mathbf{u}} \tag{3.19}$$

So, the system behavior is similar to the unconstrained problem when the calculated u_{i} is within bounds and it is capped at the limits otherwise.

3.4 Simulation

To demonstrate the above formulation, a numerical simulation has been conducted using MATLAB®. A formation comprising three spacecraft agents has been considered. These agents are initially located a specific distance d_s apart on the reference circular orbit. In the LVLH frame this appears as a straight line parallel to the y-axis. The target configuration is an equilateral triangle. It is assumed that the first agent is a 'leader', i.e., it remains on its original path. The other two agents adjust their trajectory to achieve the target final configuration with respect to the leader. Considering this communication profile, the initial and final conditions of the agents are

$$\delta\mathbf{x}_1(0) = \begin{pmatrix} 0 \\ 0 \\ 0 \\ 0 \\ 0 \\ 0 \end{pmatrix} \qquad \delta\mathbf{x}_1(t_f) = \begin{pmatrix} 0 \\ 0 \\ 0 \\ 0 \\ 0 \\ 0 \end{pmatrix} \tag{3.20}$$

$$\delta\mathbf{x}_2(0) = \begin{pmatrix} 0 \\ d_s \\ 0 \\ 0 \\ 0 \\ 0 \end{pmatrix} \qquad \delta\mathbf{x}_2(t_f) = \begin{pmatrix} -d_s \cos 60^o \\ d_s \sin 60^o \\ 0 \\ 0 \\ 0 \\ 0 \end{pmatrix} \tag{3.21}$$

$$\delta\mathbf{x}_3(0) = \begin{pmatrix} 0 \\ 2d_s \\ 0 \\ 0 \\ 0 \\ 0 \end{pmatrix} \qquad \delta\mathbf{x}_3(t_f) = \begin{pmatrix} d_s \cos 60^o \\ d_s \sin 60^o \\ 0 \\ 0 \\ 0 \\ 0 \end{pmatrix} \tag{3.22}$$

For this example a geostationary reference orbit has been considered, which means $\omega = 2\pi$ rad/day $\approx 7.2722 \times 10^{-5}$ rad/s. The reconfiguration time t_f is 30 minutes. The separation distance d_s is taken as 5% of the orbital radius, which means $d_s = 21.1205$ km. The maximum admissible magnitude of control input i.e., $U = 3 \times 10^{-5}$ km/s^2.

Using these conditions, the problem has been simulated. MATLAB®'s built-in *bvp4c* function has been used to solve the boundary value problem. The total cost is $J = 8.9028 \times 10^{-7}$ km^2/s^3. The trajectory of the agents and the control history have been plotted below in Fig. (3.1) and Fig. (3.2) respectively.

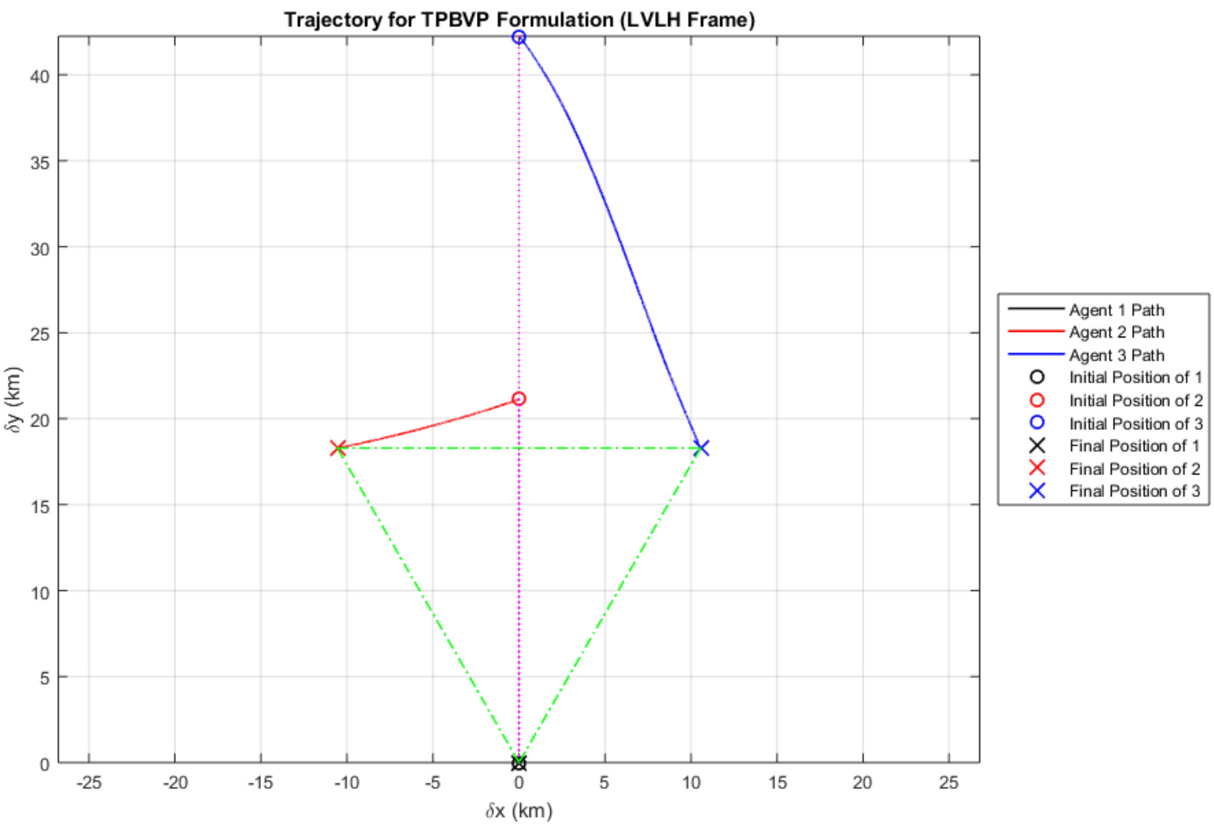

Figure 3.1. Trajectory of the Agents in the TPBVP Formulation

It is observed that the shape reconfiguration is completed successfully while implementing the control bounds. The cost for various reconfiguration times for this model has been listed in Table (3.2). It is observed that the cost decreases when t_f is increased, i.e. the longer the reconfiguration time, the lower the cost.

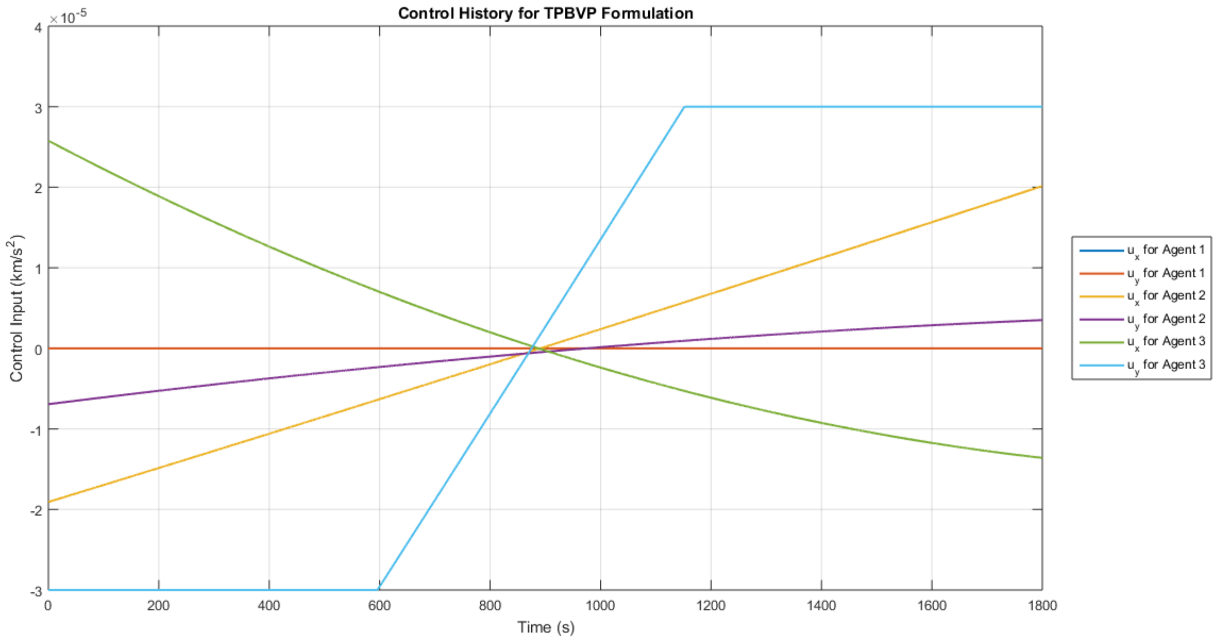

Figure 3.2. Control History in the TPBVP Formulation

Table 3.2. Cost for Different Reconfiguration Times

Reconfiguration Time t_f (s)	**Cost J (km^2/s^3)**
1800	8.9028×10^{-7}
3600	1.0536×10^{-7}
7200	1.3778×10^{-8}
18000	1.1181×10^{-9}
36000	3.3696×10^{-10}

3.5 Drawbacks of the BVP Formulation

Although this formulation works, as demonstrated above, there are some major drawbacks associated with this type of methods that limit their use in space applications. Some of these issues are as follows:

1. The exact initial and final states (i.e., both position and velocity) must be known for each agent.

2. The computation time increases with number of agents. Thus the problem does not scale well for large formations.

3. The number of iterations required for convergence depends on the initial guess for the solution. However, this guess also includes the co-states, which may not always be intuitive.

4. The applied control is specific to the dynamical equation used in the formulation. Thus, the presence of disturbances in a real scenario will result in errors.

Some of these challenges can be overcome using a closed-loop control. This has been demonstrated in the next chapter.

4. CLOSED-LOOP FORMULATION

In this chapter, the shape reorganization problem is presented as a distributed closed-loop multi-agent control problem wherein each agent receives information from its neighbors and combines these with its own. The control of each agent therefore takes into account the state of the agent as well as the states of its immediate neighbors. The exact final state of each agent does not need to be specified in this problem. It is sufficient to know only the relative positions of the agents in the desired final shape. This formulation attempts to eliminate some of the shortcomings of the TPBVP formulation in Chapter 3.

Since this formulation involves information sharing, a brief discussion of a few aspects of graph theory is necessary in order to understand the problem.

4.1 Notes on Algebraic Graph Theory

For a directed graph (digraph) with n nodes, the set of possible edges $\mathcal{E}$ is of size $n \times n$. $\mathcal{N}_{\mathrm{i}}$ denotes the set of neighbors of the i^{th} node, comprising all the other nodes from which the i^{th} node receives information. The Laplacian of the communication graph is $L_G = [l_{\mathrm{ij}}]$, where each element is defined as

$$l_{\mathrm{ij}} = \begin{cases} -1, & \mathrm{j} \in \mathcal{N}_{\mathrm{i}} \\ |\mathcal{N}_{\mathrm{i}}|, & \mathrm{j} = \mathrm{i} \end{cases} \tag{4.1}$$

Here $|\mathcal{N}_{\mathrm{i}}|$ denotes the number of neighbors of the i^{th} node. All row-sums of L_G become zero, resulting in a zero eigenvalue, with the ones vector as its corresponding eigenvector.

An important theorem related to the graph Laplacian is the Gershgorin's Circle Theorem, which can be used to prove that for a digraph with n nodes, all non-zero eigenvalues of L_G have positive real part less than or equal to $2(n-1)$.

A graph is said to have a rooted directed spanning tree if there is at least one vertex in the graph from which there is a directed path to every other vertex in the graph.

4.2 Closed-Loop Problem Formulation

With the above insight on graph theory, the problem may now be analyzed in a new light. Similar to the TPBVP formulation, the concatenated state and input vectors have been used to formulate this problem as well. Therefore the dynamical equation for a single agent is given by the Clohessy-Wiltshire equations. For the whole formation, the dynamics may be defined by an extension of the CW equations.

$$\dot{\tilde{\mathbf{x}}} = A_f \tilde{\mathbf{x}} + B_f \tilde{\mathbf{u}} \tag{4.2}$$

Here, $\tilde{\mathbf{x}}$ and $\tilde{\mathbf{u}}$ are the concatenated state and control, $A_f = I_n \otimes A$ and $B_f = I_n \otimes B$, A and B are the system and control matrices from the state space representation of the CW equations.

The target shape to which the formation shall reconfigure must be stated. A reference configuration for this target may be represented as a vector $\mathbf{h}$. For an n-agent formation, this vector takes the following form.[16]

$$\mathbf{h} = \begin{bmatrix} \mathbf{h}_1 \\ 0_{3\times1} \\ \mathbf{h}_2 \\ 0_{3\times1} \\ \vdots \\ \mathbf{h}_n \\ 0_{3\times1} \end{bmatrix} = \begin{bmatrix} \mathbf{h}_{\mathrm{i}} \\ 0_{3\times1} \end{bmatrix}_{\mathrm{i}=1,2,\,\dots\,,n} = \begin{bmatrix} \bar{\mathbf{h}}_{\mathrm{i}} \end{bmatrix}_{\mathrm{i}=1,2,\,\dots\,,n} \tag{4.3}$$

Here, $\mathbf{h}_{\mathrm{i}}$ contains the position of the i^{th} vertex of the target shape in a moving coordinate frame, i.e. $\mathbf{h}_{\mathrm{i}} = [x_{h\mathrm{i}} \quad y_{h\mathrm{i}} \quad z_{h\mathrm{i}}]^T$.

When the agents are in a specific formation, conducting a coordinated activity, they must reach a velocity consensus, which means that the relative velocity of any pair of agents in the formation must be zero. Hence the velocities in the $\mathbf{h}$ vector are 0.

It is to be noted that $\mathbf{h}$ only specifies the relative positions and velocities of each spacecraft. Therefore, the actual final position of the i^{th} spacecraft may not be $\mathbf{h}_\mathrm{i}$. However, upon convergence, the difference $\delta \mathbf{x}_\mathrm{i} - \bar{\mathbf{h}}_\mathrm{i} = [p \quad 0_{3\times 1}]^T, \quad \forall \mathrm{i} = 1, 2, \ldots, n$, where p is a 3×1 constant vector. So the formation converges to the exact shape that is defined by $\mathbf{h}$, but not necessarily the same coordinates. This is illustrated in Fig. (4.1).

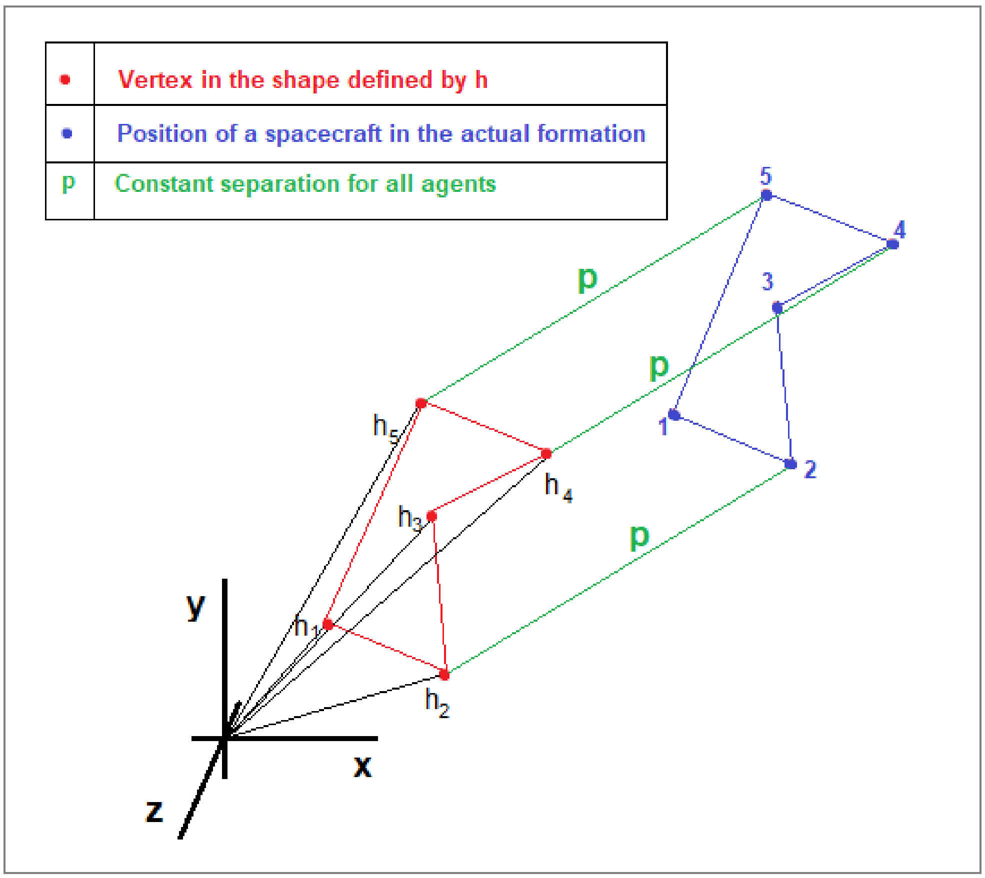

Figure 4.1. Target Shape

To combine the relative information of various agents, an 'output' term is defined, which takes the information of all the neighbors of the agent. For the i^{th} spacecraft, the information is $\delta \mathbf{x}_\mathrm{i} - \mathbf{h}_\mathrm{i}$ and the set of its neighbors is $\mathcal{N}_\mathrm{i}$. Therefore, the output term is

$$\mathbf{y}_{\mathrm{i}} = \sum_{\mathrm{j}\in N_{\mathrm{i}}} (\delta\mathbf{x_i} - \mathbf{h_i}) - (\delta\mathbf{x_j} - \mathbf{h_j}) \tag{4.4}$$

Let L_G be the communication graph Laplacian for this formation and $L_f = L_G \otimes I_6$ (since there are 6 states). Therefore, output equation for the entire formation is

$$\mathbf{y} = L_f(\tilde{\mathbf{x}} - \mathbf{h}) \tag{4.5}$$

Let K_f be a feedback matrix of the form $K_f = I_n \otimes K$ let and $\tilde{\mathbf{u}}_r$ be a reference input, such that the stacked control input is

$$\tilde{\mathbf{u}} = K_f\mathbf{y} - \tilde{\mathbf{u}}_r = \tilde{\mathbf{u}}_c - \tilde{\mathbf{u}}_r \tag{4.6}$$

$$\implies \delta\mathbf{u}_{\mathrm{i}} = K\mathbf{y}_{\mathrm{i}} - \delta\mathbf{u}_{r,\mathrm{i}} = \delta\mathbf{u}_{c,\mathrm{i}} - \delta\mathbf{u}_{r,\mathrm{i}} \tag{4.7}$$

Here $\tilde{\mathbf{u}}_c = K_f\mathbf{y} = K_f L(\tilde{\mathbf{x}} - \mathbf{h})$ may be termed as the consensus input. The reference input $\tilde{\mathbf{u}}_r$ is included in order to ensure convergence to the desired shape.

For a single agent, the CW equations can now be written as

$$\delta\ddot{x} = 2\omega\delta\dot{y} + 3\omega^2\delta x + u_{c,x} - u_{r,x} \tag{4.8a}$$

$$\delta\ddot{y} = -2\omega\delta\dot{x} + u_{c,y} - u_{r,y} \tag{4.8b}$$

$$\delta\ddot{z} = -\omega^2\delta z + u_{c,z} - u_{r,z} \tag{4.8c}$$

If the reference input components are selected as $u_{r,x} = 3\omega^2\delta x,\ u_{r,y} = 0,\ u_{r,x} = -\omega^2\delta z$, then the acceleration becomes independent of the position when the consensus input is zero. In this case, the reference input for a single agent can be represented as $\delta u_r = W\delta\mathbf{x}$, where

$$W = \begin{bmatrix} 3\omega^2 & 0 & 0 & 0 & 0 & 0 \\ 0 & 0 & 0 & 0 & 0 & 0 \\ 0 & 0 & -\omega^2 & 0 & 0 & 0 \end{bmatrix}$$

The dynamics of one agent can now be rewritten as

$$\delta\dot{\mathbf{x}} = \mathcal{A}\delta\mathbf{x} + B\delta\mathbf{u}_c \tag{4.9}$$

where,

$$\mathcal{A} = \begin{bmatrix} 0 & 0 & 0 & 1 & 0 & 0 \\ 0 & 0 & 0 & 0 & 1 & 0 \\ 0 & 0 & 0 & 0 & 0 & 1 \\ 0 & 0 & 0 & 0 & 2\omega & 0 \\ 0 & 0 & 0 & -2\omega & 0 & 0 \\ 0 & 0 & 0 & 0 & 0 & 0 \end{bmatrix} \quad B = \begin{bmatrix} 0 & 0 & 0 \\ 0 & 0 & 0 \\ 0 & 0 & 0 \\ 1 & 0 & 0 \\ 0 & 1 & 0 \\ 0 & 0 & 1 \end{bmatrix} \quad \delta\mathbf{x} = \begin{bmatrix} \delta x \\ \delta y \\ \delta z \\ \delta\dot{x} \\ \delta\dot{y} \\ \delta\dot{z} \end{bmatrix} \quad \delta\mathbf{u}_c = \begin{bmatrix} u_{c,x} \\ u_{c,y} \\ u_{c,z} \end{bmatrix}$$

Let $W_f = (I_n \otimes W)$, $\mathcal{A}_f = (I_n \otimes \mathcal{A})$ and $B_f = (I_n \otimes B)$. Therefore, the concatenated reference input can be written as

$$\tilde{\mathbf{u}}_r = W_f\tilde{\mathbf{x}} \tag{4.10}$$

The dynamics of the formation as a whole can be represented as

$$
\begin{aligned}
&\dot{\tilde{\mathbf{x}}} = \mathcal{A}_f\tilde{\mathbf{x}} + B_f\tilde{\mathbf{u}}_c \\
\implies &\dot{\tilde{\mathbf{x}}} = \mathcal{A}_f\tilde{\mathbf{x}} + B_fK_f\mathbf{y} \\
\implies &\dot{\tilde{\mathbf{x}}} = \mathcal{A}_f\tilde{\mathbf{x}} + B_fK_fL_f(\tilde{\mathbf{x}} - \mathbf{h}) \\
\implies &\dot{\tilde{\mathbf{x}}} = (\mathcal{A}_f + B_fK_fL)\tilde{\mathbf{x}} - B_fK_fL_f\mathbf{h}
\end{aligned} \tag{4.11}
$$

This can also be written as

$$
\begin{aligned}
\implies &\dot{\tilde{\mathbf{x}}} = (\mathcal{A}_f + B_fK_fL_f)\tilde{\mathbf{x}} - (\mathcal{A}_f + B_fK_fL_f)\mathbf{h} + \mathcal{A}_f\mathbf{h} \\
\implies &\dot{\tilde{\mathbf{x}}} = (\mathcal{A}_f + B_fK_fL_f)(\tilde{\mathbf{x}} - \mathbf{h}) + \mathcal{A}_f\mathbf{h}
\end{aligned} \tag{4.12}
$$

Equation (4.12) represents the dynamics in terms of $(\tilde{\mathbf{x}} - \mathbf{h})$, which may be regarded as an error term. It is to be noted that for any agent,

$$
\mathcal{A}\bar{\mathbf{h}}_{\mathrm{i}} = \begin{bmatrix} 0 & 0 & 0 & 1 & 0 & 0 \\ 0 & 0 & 0 & 0 & 1 & 0 \\ 0 & 0 & 0 & 0 & 0 & 1 \\ 0 & 0 & 0 & 0 & 2\omega & 0 \\ 0 & 0 & 0 & -2\omega & 0 & 0 \\ 0 & 0 & 0 & 0 & 0 & 0 \end{bmatrix} \begin{bmatrix} x_{h\mathrm{i}} \\ y_{h\mathrm{i}} \\ z_{h\mathrm{i}} \\ 0 \\ 0 \\ 0 \end{bmatrix} = \begin{bmatrix} 0 \\ 0 \\ 0 \\ 0 \\ 0 \\ 0 \end{bmatrix}
$$

Therefore,

$$\mathcal{A}_f\mathbf{h} = \begin{bmatrix} \mathcal{A} & 0 & \dots & 0 \\ 0 & \mathcal{A} & \dots & 0 \\ \vdots & \vdots & \ddots & \vdots \\ 0 & 0 & \dots & \mathcal{A} \end{bmatrix} \begin{bmatrix} \bar{\mathbf{h}}_1 \\ \bar{\mathbf{h}}_2 \\ \vdots \\ \bar{\mathbf{h}}_n \end{bmatrix} = \begin{bmatrix} \mathcal{A}\bar{\mathbf{h}}_1 \\ \mathcal{A}\bar{\mathbf{h}}_2 \\ \vdots \\ \mathcal{A}\bar{\mathbf{h}}_n \end{bmatrix} = \begin{bmatrix} 0 \\ 0 \\ \vdots \\ 0 \end{bmatrix} \tag{4.13}$$

So, the effective system dynamics can be written as

$$\dot{\tilde{\mathbf{x}}} = (\mathcal{A}_f + B_f K_f L_f)(\tilde{\mathbf{x}} - \mathbf{h}) \tag{4.14}$$

It has been proven by Ren et al. [17] that the above system converges to the formation $\mathbf{h}$ if and only if $(\mathcal{A}_f + B_f K_f L_f)$ has eigenvalues with non-positive real parts and the communication graph G has a rooted directed spanning tree. This means that the Laplacian L_G must have zero as an eigenvalue with algebraic multiplicity 1.

From equation (4.11) it can be concluded that the stability of the system depends on the matrix $\mathcal{A}_f + B_f K_f L_f$. Based on the way the $\mathcal{A}_f, B_f, K_f$ and L_f matrices have been defined, this can be reduced to the following form.

$$\begin{aligned} \mathcal{A}_f + B_f K_f L_f &= (I_n \otimes \mathcal{A}) + (I_n \otimes B)(I_n \otimes K)(L_G \otimes I_6) \\ &= (I_n \otimes \mathcal{A}) + (I_n I_n L_G \otimes B K I_6) \\ &= (I_n \otimes \mathcal{A}) + (L_G \otimes BK) \end{aligned}$$

Let T be a non-singular matrix such that $\bar{L}_G = T^{-1} L_G T$ is upper triangular. This means that the diagonal elements of $\bar{L}_G$ are the eigenvalues of L_G, i.e. $\lambda_1, \lambda_2, \dots, \lambda_n$.

$$
\begin{aligned}
&(T^{-1} \otimes I_6)(\mathcal{A}_f + B_f K_f L_f)(T \otimes I_6) \\
=&(T^{-1} \otimes I_6)(I_n \otimes \mathcal{A} + L_G \otimes BK)(T \otimes I_6) \\
=&(T^{-1} \otimes I_6)(I_n \otimes \mathcal{A})(T \otimes I_6) + (T^{-1} \otimes I_6)(L_G \otimes BK)(T \otimes I_6) \\
=&(T^{-1} I_n T \otimes I_6 \mathcal{A} I_6) + (T^{-1} L_G T \otimes I_6 BK I_6) \\
=&(I_n \otimes \mathcal{A}) + (\bar{L}_G \otimes BK)
\end{aligned}
$$

Since , $\bar{L}_G$ and L_G have the same eigenvalues, the above matrix has the same eigenvalues as $(\mathcal{A}_f + B_f K_f L)$. Moreover, $(I_n \otimes \mathcal{A} + \bar{L}_G \otimes BK)$ is a block upper triangular $6n \times 6n$ matrix of the form

$$
(I_n \otimes \mathcal{A} + \bar{L}_G \otimes BK) = \begin{bmatrix} (\mathcal{A} + \lambda_1 BK) & \bar{l}_{12} BK & \dots & \bar{l}_{1n} BK \\ 0 & (\mathcal{A} + \lambda_2 BK) & \dots & \bar{l}_{2n} BK \\ \vdots & \vdots & \ddots & \vdots \\ 0 & 0 & \dots & (\mathcal{A} + \lambda_n BK) \end{bmatrix} \tag{4.15}
$$

Therefore, the eigenvalues of $(\mathcal{A}_f + B_f K_f L)$ are the eigenvalues of $(\mathcal{A} + \lambda_\mathrm{i} BK)$ $\forall \mathrm{i} = 1, 2, \dots, n$, where λ_i is the i^{th} eigenvalue of L_G. The system converges to the desired formation if $(\mathcal{A} + \lambda BK)$ is Hurwitz for all non-zero eigenvalues λ of L_G. In other words, the feedback K is a stabilizing feedback if and only if makes $(\mathcal{A} + \lambda BK)$ Hurwitz for all non-zero eigenvalues λ of L_G.

4.3 Main Result: Stabilizing Feedback Gain

In order to stabilize the system and drive it to the desired formation, a feedback-based controller has been designed. The feedback gain for this controller is a multiple of an LQR feedback gain which is known to yield a stable system.

4.3.1 Solution Approach

The dynamics of the ith agent in the formation is represented as $\delta\dot{\mathbf{x}} = \mathcal{A}\delta\mathbf{x} + B\delta\mathbf{u}_c$. Let K_{lqr} be the feedback gain that minimizes the linear quadratic cost

$$J_{lqr} = \int_0^{\infty} \left[(\delta\mathbf{x})^T Q(\delta\mathbf{x}) + (\delta\mathbf{u}_c)^T R(\delta\mathbf{u}_c)\right] \, dt \tag{4.16}$$

Let $R = I$ (identity) and $Q = qI$, where $q < 1$. It is to be noted that as the value of q decreases, the problem tends to a fuel optimization problem.

The K_{lqr} matrix is used as the feedback matrix for all agents in the formation. This always results in a stable system matrix $\mathcal{A} + BK_{lqr}$ that has eigenvalues with negative real parts.

4.3.2 Theorem

Let the Hermitian matrix P be the stabilizing solution to the Algebraic Riccati equation, $P\mathcal{A} + \mathcal{A}P - PBR^{-1}BP + Q = 0$, Q and R being the weight matrices in the LQR cost in equation (4.16). Therefore, the feedback gain K_{lqr} is given by

$$K_{lqr} = -R^{-1}BP \tag{4.17}$$

It is proposed that a multiple of the above gain matrix, γK_{lqr} can stabilize the system $\mathcal{A} + \lambda B(\gamma K_{lqr})$ when γ lies within a specific range.

Theorem: *$\mathcal{A} + \lambda BK$ is Hurwitz for all non-zero eigenvalues λ of L_G if $K = \gamma K_{lqr}$, and γ is greater than or equal to one-half of the reciprocal of the minimum real part of the non-zero eigenvalues of L_G.*

4.3.3 Proof of Theorem

$K_f = I_n \otimes (\gamma K_{lqr})$ is used as stabilizing feedback matrix for the whole formation. This requires the matrix $\mathcal{A} + \lambda B(\gamma K_{lqr})$ to be Hurwitz for all non-zero eigenvalues λ of the graph Laplacian L_G. The goal is to find the values of γ that will ensure that this criterion is satisfied. To obtain this value, a system is considered, the dynamics for which can be written as $\dot{\chi} = (\mathcal{A} + \lambda BK)\chi = (\mathcal{A} + \lambda\gamma BK_{lqr})\chi = \bar{\mathcal{A}}\chi$, where χ is the state vector for this system and λ is a non-zero eigenvalue of L_G.

Let a Lyapunov function $V(\chi(t))$ be defined as

$$V(\chi(t)) = \chi'(t)P\chi(t) \tag{4.18}$$

Taking derivative with respect to time yields

$$\begin{aligned}
\frac{dV}{dt} &= \chi'P\dot{\chi} + \dot{\chi}'P\chi &\quad (4.19)\\
&= \chi'P\bar{\mathcal{A}}\chi + \chi'\bar{\mathcal{A}}'P\chi \\
&= \chi'P(\mathcal{A} + \lambda\gamma BK_{lqr})\chi + \chi'(\mathcal{A} + \lambda\gamma BK_{lqr})'P\chi \\
&= \chi'[P\mathcal{A} + \lambda\gamma PBK_{lqr} + \mathcal{A}'P + \bar{\lambda}\gamma(K'_{lqr}B'P)]\chi \\
\implies \frac{dV}{dt} &= \chi'[P\mathcal{A} + \lambda\gamma PBK_{lqr} + \mathcal{A}'P + \bar{\lambda}\gamma(PBK_{lqr})']\chi &\quad (4.20)
\end{aligned}$$

P solves the Algebraic Riccati Equation, $P\mathcal{A} + \mathcal{A}'P - PBR^{-1}B'P + Q = 0$. Therefore, $P\mathcal{A} + \mathcal{A}'P = PBR^{-1}B'P - Q = PBB'P - Q$ (since $R = I$).

From equation (4.17), $PBK_{lqr} = -PBR^{-1}B'P = -PBIB'P = -PBB'P$. So,

$$\frac{dV}{dt} = \chi'[PBB'P - Q + \gamma\{\lambda(-PBB'P) + \bar{\lambda}(-PBB'P)'\}]\chi \tag{4.21}$$

The following two matrix properties are required for the further analysis of the system.

Property 1: For any matrix M, the products $M'M$ and MM' are Hermitian positive semi-definite.

Property 2: If U is a positive semi-definite matrix, then $T'UT$ is also positive semi-definite for any matrix T.

Using the above-mentioned properties (taking $M = B$, $U = BB'$ and $T = P = T'$) it can be concluded that BB' and $PBB'P$ are Hermitian positive semi-definite. This means $(PBB'P)' = PBB'P$. Therefore,

$$
\begin{aligned}
\frac{dV}{dt} &= \chi'[PBB'P - Q - \gamma(\lambda + \bar{\lambda})PBB'P]\chi \\
&= \chi'[PBB'P - Q - 2\gamma\,\mathrm{Re}(\lambda)PBB'P]\chi \\
&= \chi'[PBB'P\{1 - 2\gamma\,\mathrm{Re}(\lambda)\}]\chi - \chi'(Q)\chi \\
\implies \frac{dV}{dt} &= \{1 - 2\gamma\,\mathrm{Re}(\lambda)\}\chi'(PBB'P)\chi - \chi'(Q)\chi \qquad (4.22)
\end{aligned}
$$

For stability, the necessary condition is $\frac{dV}{dt} < 0$. Therefore,

$$
\{1 - 2\gamma\,\mathrm{Re}(\lambda)\}\chi'(PBB'P)\chi - \chi'(Q)\chi < 0 \qquad (4.23)
$$

For our system, $Q = qI$, $0 < q << 1$, i.e. Q is positive definite and $\chi'Q\chi > 0 \implies -\chi'Q\chi < 0$. Moreover, $PBB'P$ is positive semi-definite, so $\chi'PBB'P\chi \geq 0$. Therefore, the system is guaranteed to be stable if

$$
\begin{aligned}
\{1 - 2\gamma\,\mathrm{Re}(\lambda)\} &\leq 0 \qquad (4.24) \\
\implies \gamma &\geq \frac{1}{2\,\mathrm{Re}(\lambda)}, \qquad \forall \lambda \in \sigma(L_G), \lambda \neq 0 \qquad (4.25)
\end{aligned}
$$

Here $\sigma(L_G)$ represents the spectrum of L_G. Using Gershgorin's Circle Theorem, it can be derived that the non-zero eigenvalues of L_G all have positive real parts. Let λ_i be the non-zero eigenvalues of L_G, such that $\mathrm{Re}(\lambda_1) < \mathrm{Re}(\lambda_2) < \cdots < \mathrm{Re}(\lambda_{n-1})$. As $\mathrm{Re}(\lambda_\mathrm{i}) > 0 \quad \forall \mathrm{i} = 1, 2, \ldots n-1$, the reciprocals are related as $\frac{1}{\mathrm{Re}(\lambda_1)} > \frac{1}{\mathrm{Re}(\lambda_2)} > \cdots > \frac{1}{\mathrm{Re}\,\lambda_{n-1}}$.

Therefore, for γ to satisfy the condition in equation (4.25), $\gamma \geq \frac{1}{2\,\mathrm{Re}\,\lambda_1}$, i.e.

$$
\gamma \geq \frac{1}{2\,\mathrm{Re}(\lambda)_{min}} \qquad (4.26)
$$

i.e. γ is greater than or equal to one-half of the reciprocal of the minimum real part of the non-zero eigenvalues of L_G.

Therefore, when γ satisfies equation (4.26), the matrix feedback matrix $K = \gamma K_{lqr}$ makes $A + \lambda BK$ Hurwitz for all nonzero eigenvalues λ of the graph Laplacian L_G. The proposed theorem is thus proved to be true.

4.4 Simulation

To demonstrate the effectiveness of the controller derived in this chapter, a simulation has been conducted using MATLAB®, with the same parameters as the example in the TPBVP formulation. The three-spacecraft formation is in a geostationary reference orbit ($\omega = 2\pi$ rad/day). The initial configuration is a straight line in the LVLH frame with a separation distance of $d_s = 21.1205$ km. The final configuration is an equilateral triangle of side length d_s. The target configuration is

$$h = \begin{pmatrix} \bar{h}_1 \\ \bar{h}_2 \\ \bar{h}_3 \end{pmatrix} \quad \text{where,} \quad \bar{h}_1 = \begin{pmatrix} 0 \\ 0 \\ 0 \\ 0 \\ 0 \\ 0 \end{pmatrix} \qquad \bar{h}_2 = \begin{pmatrix} -d_s \cos 60^o \\ d_s \sin 60^o \\ 0 \\ 0 \\ 0 \\ 0 \end{pmatrix} \qquad \bar{h}_3 = \begin{pmatrix} d_s \cos 60^o \\ d_s \sin 60^o \\ 0 \\ 0 \\ 0 \\ 0 \end{pmatrix}$$

A function is used to apply a bound on the control, such that its magnitude is less than $U = 1 \times 10^{-4}$ km/s^2. The communication graph is directed as Agent1 $\rightarrow$ Agent2 $\rightarrow$ Agent3, making Agent1 the leader. The Laplacian is therefore,

$$L_G = \begin{bmatrix} 0 & 0 & 0 \\ -1 & 1 & 0 \\ 0 & -1 & 1 \end{bmatrix} \tag{4.27}$$

The eigenvalues of L_G are 0, 1, 1. So, $\gamma \geq 0.5$. A value of $\gamma = 3$ has been selected. In this example, $q = 10^{-9}$.

Using these values, the calculated feedback gain is

$$K = \begin{bmatrix} -0.0000949 & 0.0000017 & 0 & -0.0238563 & 0 & 0 \\ -0.0000017 & -0.0000949 & 0 & 0 & -0.0238563 & 0 \\ 0 & 0 & -0.0000949 & 0 & 0 & -0.0238563 \end{bmatrix} \tag{4.28}$$

The system has been simulated using MATLAB® and Simulink®. The trajectory of the agents and the control history have been plotted in Fig. (4.2) and Fig. (4.3) respectively. It is observed that the reconfiguration procedure is successfully completed, thus validating the controller derived above.

If the leader is given an initial velocity, the whole system moves in formation with respect to the LVLH frame. This is shown in Fig. (4.4) for the leader's initial velocity $(\dot{x}, \dot{y}, \dot{z}) =$ (0.01, 0.03, 0) km/s, keeping all other parameters the same.

The next chapter demonstrates the potential practical applications of the shape reorganization problem and the use of this controller in such applications.

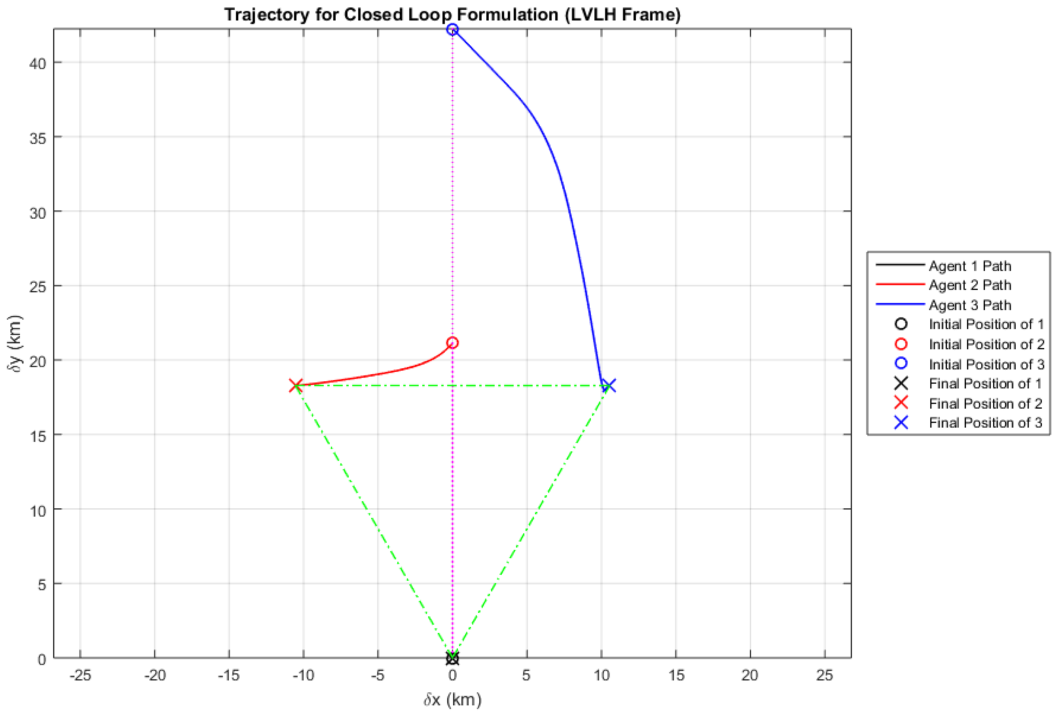

Figure 4.2. Trajectory of the Agents in the Closed-Loop Formulation

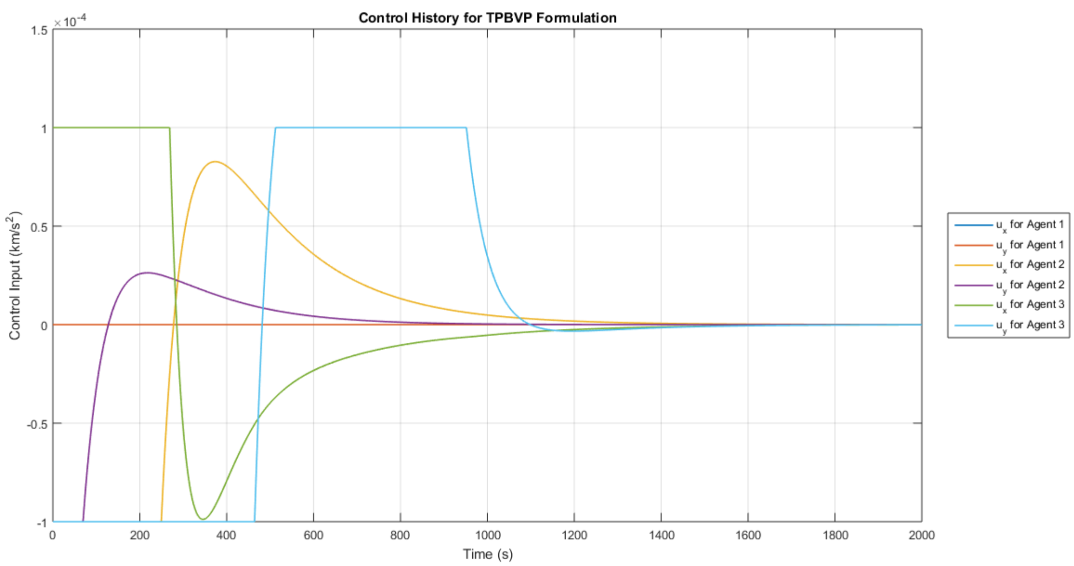

Figure 4.3. Control History in the Closed-Loop Formulation

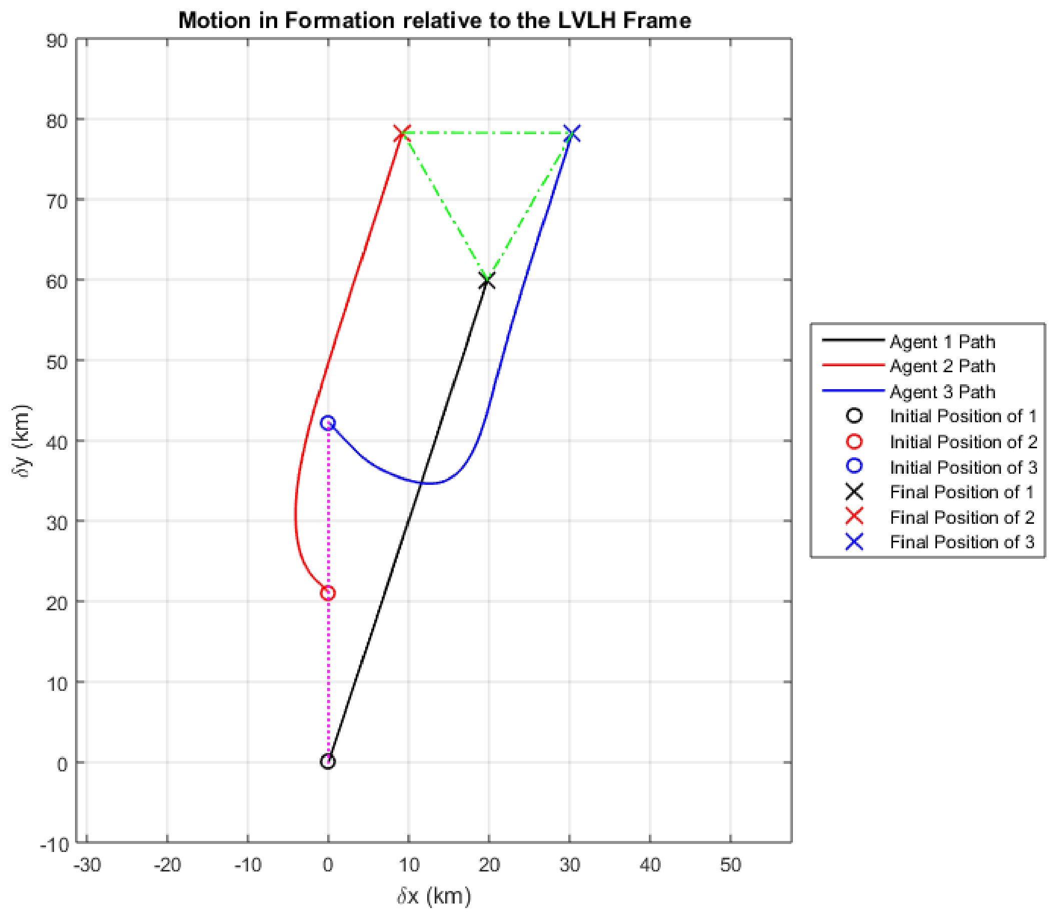

Figure 4.4. System Moving in Formation

5. POTENTIAL APPLICATIONS

The applications of the shape reconfiguration problem are illustrated in this chapter. In the last few years, several projects have been proposed worldwide that involve spacecraft clusters, constellations, or formations. For most of these applications, the ability of spatial reorientation can substantially expand their scope of operation. This capability can also improve the overall reliability of the system by increasing component redundancy and providing the opportunity for easy replacement in case of failure.

5.1 Extension of the Controller to the Nonlinear System

While the analysis and calculations in this thesis have been conducted for the linearized system as defined by the Clohessy-Wiltshire equations, the real motion of objects in outer space is nonlinear. The actual dynamics of a point mass in the two-body problem can be expressed in terms of the LVLH coordinates as

$$\ddot{x} = 2\omega\dot{y} + (\omega^2 - \frac{\mu}{r^3})x + a_{p,x} + u_x \tag{5.1a}$$

$$\ddot{y} = -2\omega\dot{x} + (\omega^2 - \frac{\mu}{r^3})y + a_{p,y} + u_y \tag{5.1b}$$

$$\ddot{z} = -\frac{\mu}{r^3}z + a_{p,z} + u_z \tag{5.1c}$$

Here, a_p denotes acceleration due to perturbations. A major source of perturbations in the solar system is Solar Radiation Pressure (SRP). This occurs due to the exchange of momentum between a surface and the photons present in sunlight. The acceleration due to SRP may be defined [18] as follows.

$$a_{SRP} = \frac{S\,(AU)^2\,C_R\,A_{SRP}\,v}{m\,r_s^2\,c} \tag{5.2}$$

Here, S is the solar flux at one astronomical unit (generally taken as 1358 W/m^2), AU is one astronomical unit, i.e., 149,597,870.0 km, C_R is the coefficient of reflectivity, A_{SRP} is the cross sectional area incident to the sunline, v is the shadow factor (1 if in light, 0 if in complete shadow), m is the mass of the spacecraft, r_s is the distance of the spacecraft from the sun, c is the speed of light. This acceleration is in the direction of the sun-spacecraft unit vector and its component along any specific direction may be computed by the dot product of the acceleration with the unit vector in that direction.

If the formation is in orbit around a planet, the oblateness of the planet gives rise to what is known as J_2 perturbations. In the inertial frame, the components of the accelerations due to J_2 perturbations for a geocentric orbit may be defined [19] as

$$a_{Jx\mathrm{i}} = \frac{3}{2}\mu J_2 \frac{R_E^2}{r^5} r_x \left(5\left(\frac{r_z}{r}\right)^2 - 1\right) \tag{5.3a}$$

$$a_{Jy\mathrm{i}} = \frac{3}{2}\mu J_2 \frac{R_E^2}{r^5} r_y \left(5\left(\frac{r_z}{r}\right)^2 - 1\right) \tag{5.3b}$$

$$a_{Jz\mathrm{i}} = \frac{3}{2}\mu J_2 \frac{R_E^2}{r^5} r_z \left(5\left(\frac{r_z}{r}\right)^2 - 3\right) \tag{5.3c}$$

Here r_x, r_y, r_z are the inertial position coordinates. For the Earth, the constant $J_2 = 1.0826 \times 10^{-3}$. R_E is the radius of the Earth and r is the distance between the Earth and the spacecraft. These accelerations may be translated to the LVLH coordinates by multiplying with a transformation matrix.

The accelerations due to these perturbing forces in the x, y, z directions in equation (5.1) may then be represented as

$$a_{p,x} = a_{SRP,x} + a_{J2,x}$$

$$a_{p,y} = a_{SRP,y} + a_{J2,y}$$

$$a_{p,z} = a_{SRP,z} + a_{J2,z}$$

Other relevant types of perturbing forces may be included, based on the type of orbit being simulated. For example, in Low Earth Orbit, atmospheric drag causes significant deviations. Similarly, when the orbit comes close to another attracting body apart from the central body, there are perturbations due to secondary gravitational fields. These may be modeled into the nonlinear equations of motion.

The states (position and velocity) of a spacecraft at a given time are obtained by integrating equation (5.1). The equilibrium state is then subtracted from these nonlinear states and the closed-loop controller is applied to the difference. The control input thus derived is fed into the nonlinear equations. This is schematically represented in Fig. (5.1).

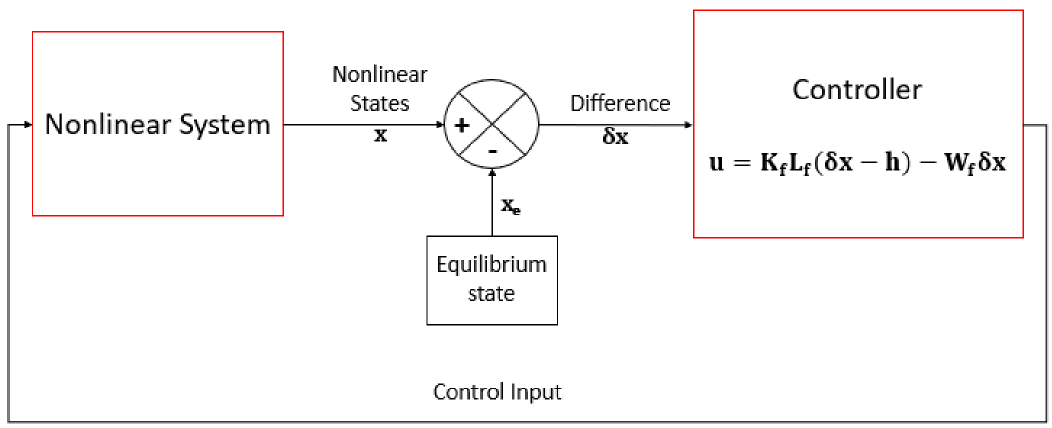

Figure 5.1. Control of the Nonlinear System

In the sections that follow, the above method has been applied to demonstrate some potential applications of this work. All simulations have been done using MATLAB® and Simulink®.

5.2 Fractionated Space Telescope

Space telescopes have helped humanity discover astounding realms in the universe and understand enigmatic phenomena such as the birth of stars and formation of galaxies. The most famous and versatile of them is the Hubble Space Telescope, which has been in operation since 1990. Its successor, the James Webb Space Telescope is currently being prepared for launch. Being massive structures, these telescopes result in a high cost of launch. Subsequent maintenance also adds to the cost. To avoid these expenses, several organizations have proposed designs of fractionated telescopes. One such design by NASA JPL serves as the motivation for this simulation.

5.2.1 Motivation

A fractionated space telescope has been proposed as a successor to the James Webb Space Telescope by Lee et al. [20]. The design comprises four separate units, namely

1. Primary Mirror

2. Sunshade

3. Optics and Instrumentation Unit (OIU)

4. Metrology Unit (MU)

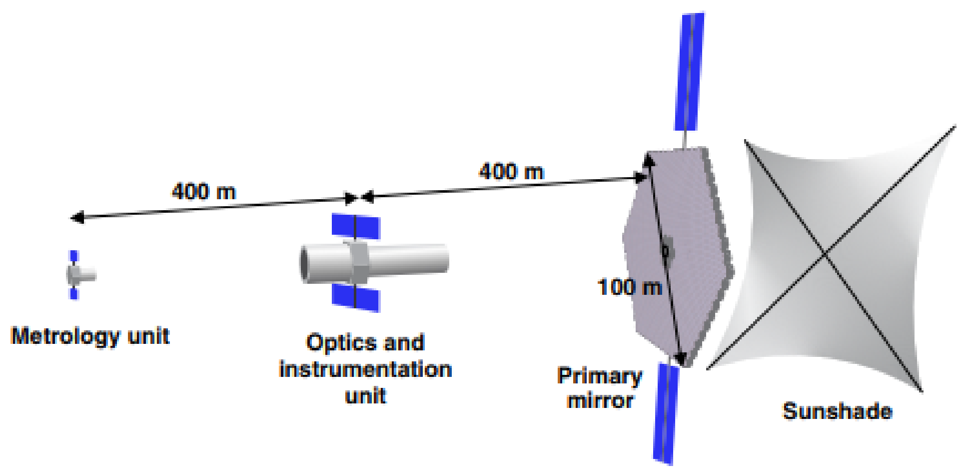

Figure 5.2. Fractionated Telescope [20]

These are shown in Fig. (5.2). Each unit is an individual spacecraft, with its own propulsion and attitude control system, and a specific function within the telescope system. Since these are mechanically separate, the units can be launched individually at a low cost. During operation, these units shall fly in formation to operate in tandem.

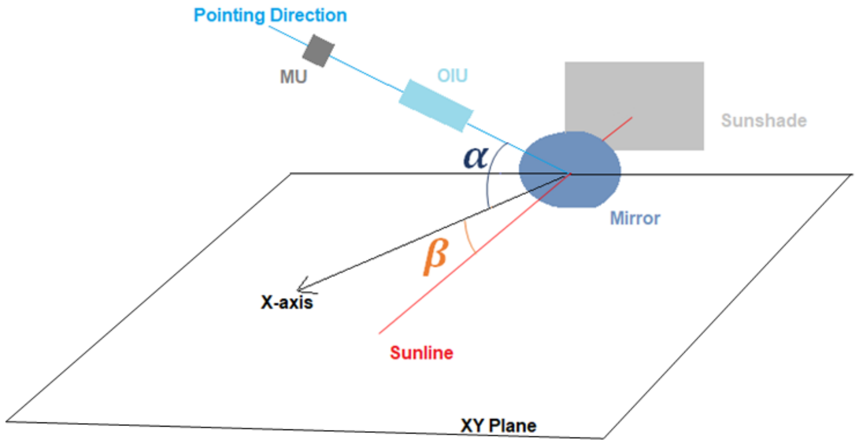

Figure 5.3. Orientation of the Telescope

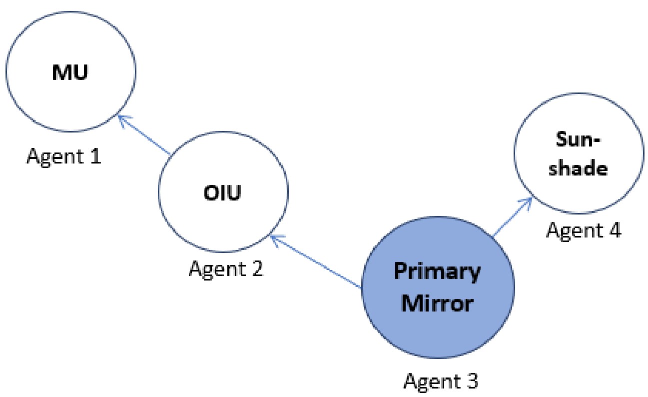

Figure 5.4. Telescope Communication Graph

5.2.2 Problem Setup

The four units in the space telescope must be aligned in a specific manner for proper operation. The primary mirror collects and focuses light from celestial bodies, which is then processed and corrected by the OIU and the MU. Therefore, these must be aligned in the direction of the celestial body that is under observation. The sunshade protects the system from the light and heat of the sun. Therefore, it must be oriented along the sunline. The relative orientation of the telescope may be described using two angles, i.e., the pointing angle α and sunline angle β. This has been illustrated in Fig (5.3).

The telescope would frequently need to change orientation depending on the relative location of the sun and the observation target. This will require shape reconfiguration capability.

An example of this kind of reconfiguration has been simulated. Here the number of agents, $n = 4$. The location of the primary mirror is the most sensitive. Therefore, the communication graph that has been considered for this simulation has the primary mirror as the leader, as shown in Fig (5.4). At the initial time, the primary mirror coincides with the equilibrium point with respect to which the CW dynamics are defined. The formation is moving in a heliocentric orbit that passes through the Sun-Earth Lagrange Point 2 (SEL2). As the central body is the Sun, J_2 perturbations do not apply here. Additionally, as the reference orbit is circular, the SRP acceleration acts along the LVLH x-direction at all times. The SRP data has been taken from Lee et al. [20].

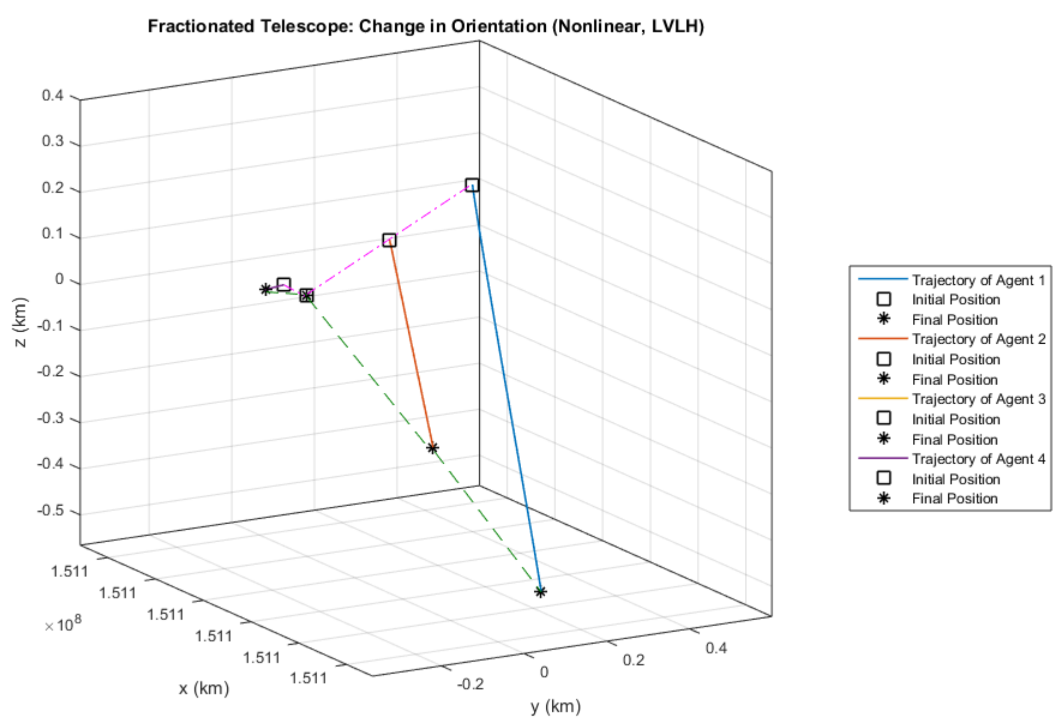

Figure 5.5. Telescope Orientation Change, LVLH Frame

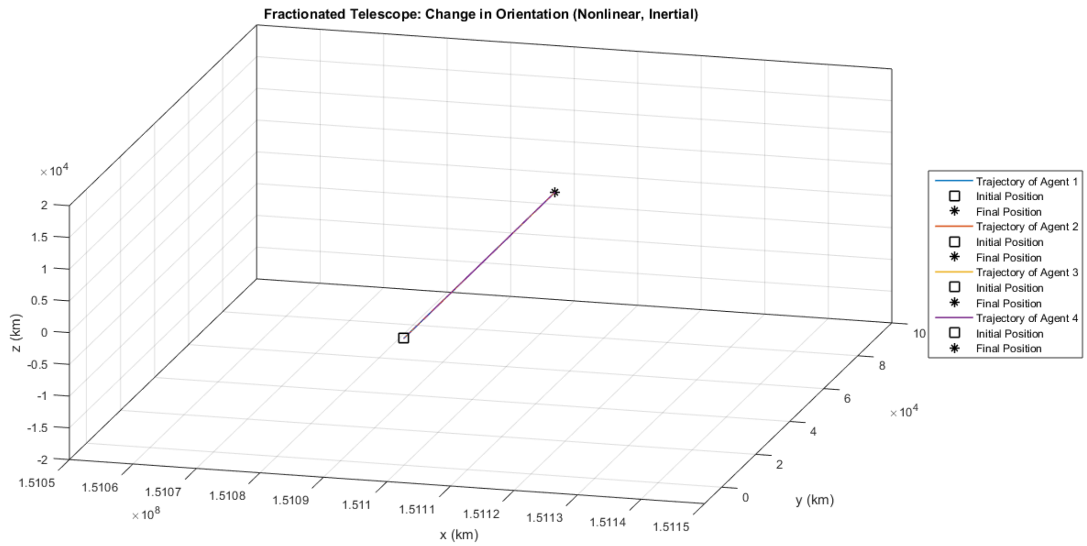

Figure 5.6. Telescope Orientation Change, Inertial Frame

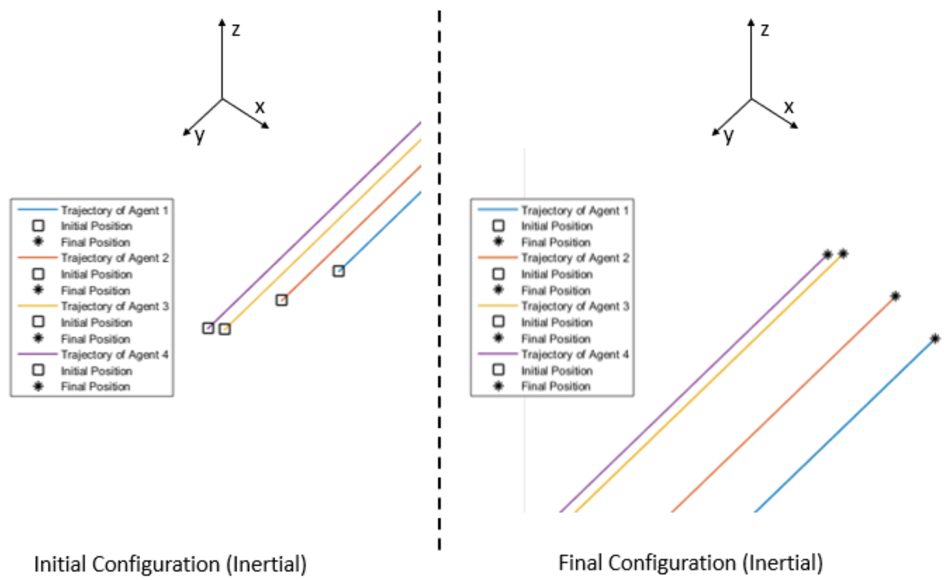

Figure 5.7. Initial and Final Configuration of the Telescope, Inertial Frame

The change of (α, β) orientation from $(30^o, 0^o)$ to $(-45^o, 15^o)$ has been simulated. The separation distances mentioned in Fig. (5.2) have been used.

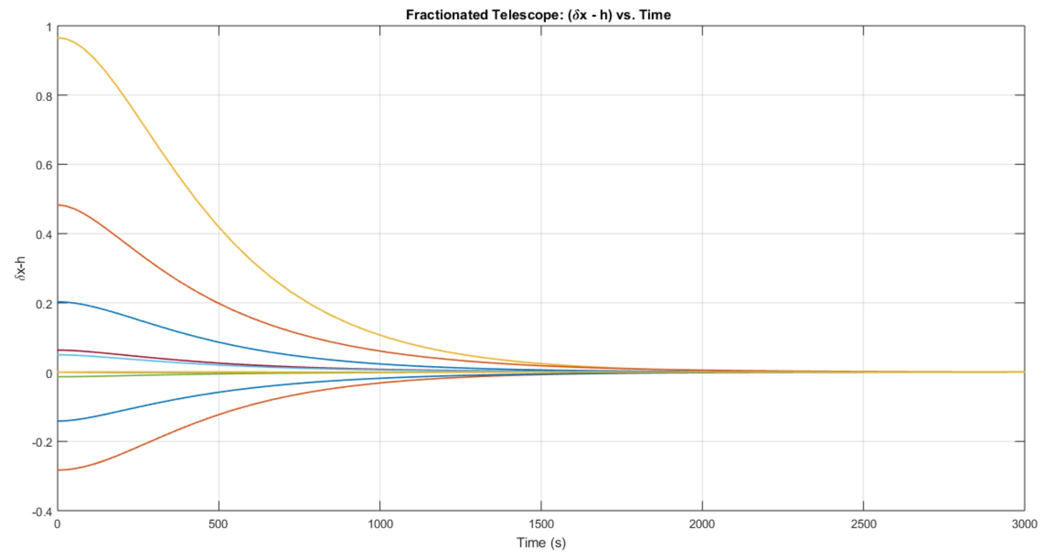

Figure 5.8. Evolution of $(\delta x - h)$ over Time for Telescope Reconfiguration

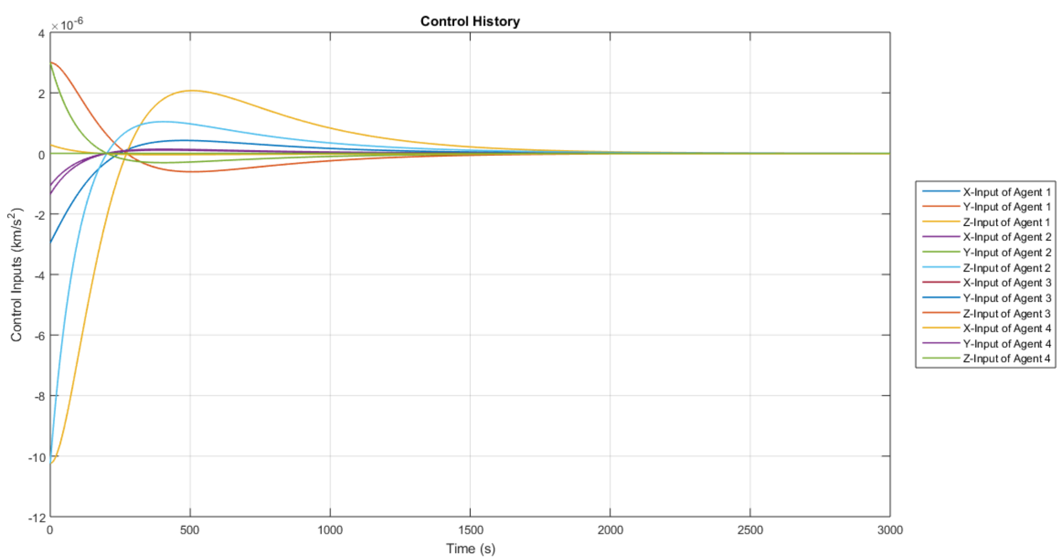

Figure 5.9. Control History of the Nonlinear System

5.2.3 Simulation Results

The reorganization of the units of the telescope in the LVLH frame has been shown in Fig. (5.5). The same procedure in the inertial frame is illustrated in Fig. (5.6). The motion of the agents along the orbit during the reconfiguration procedure is apparent here, but due

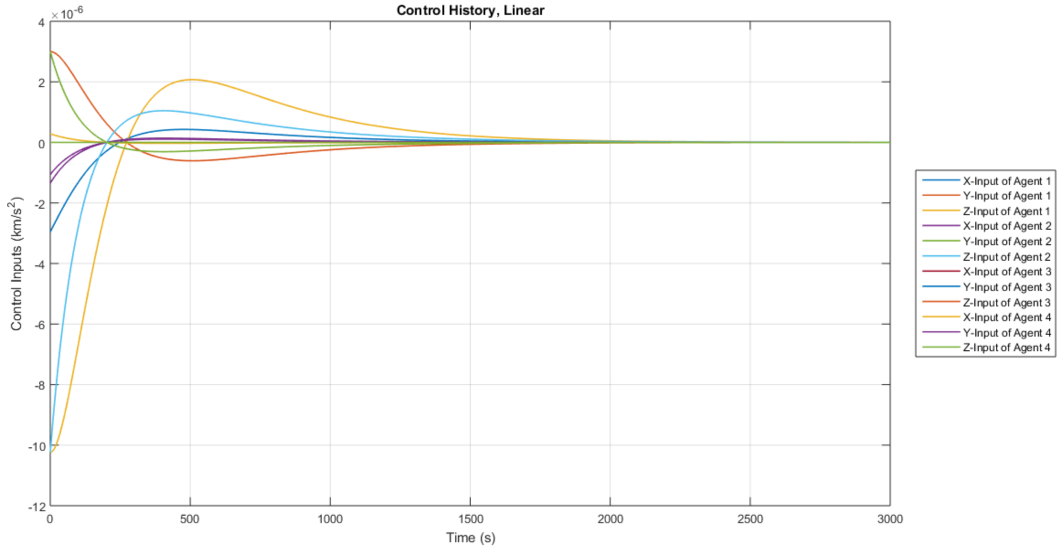

Figure 5.10. Control History of the Linearized System

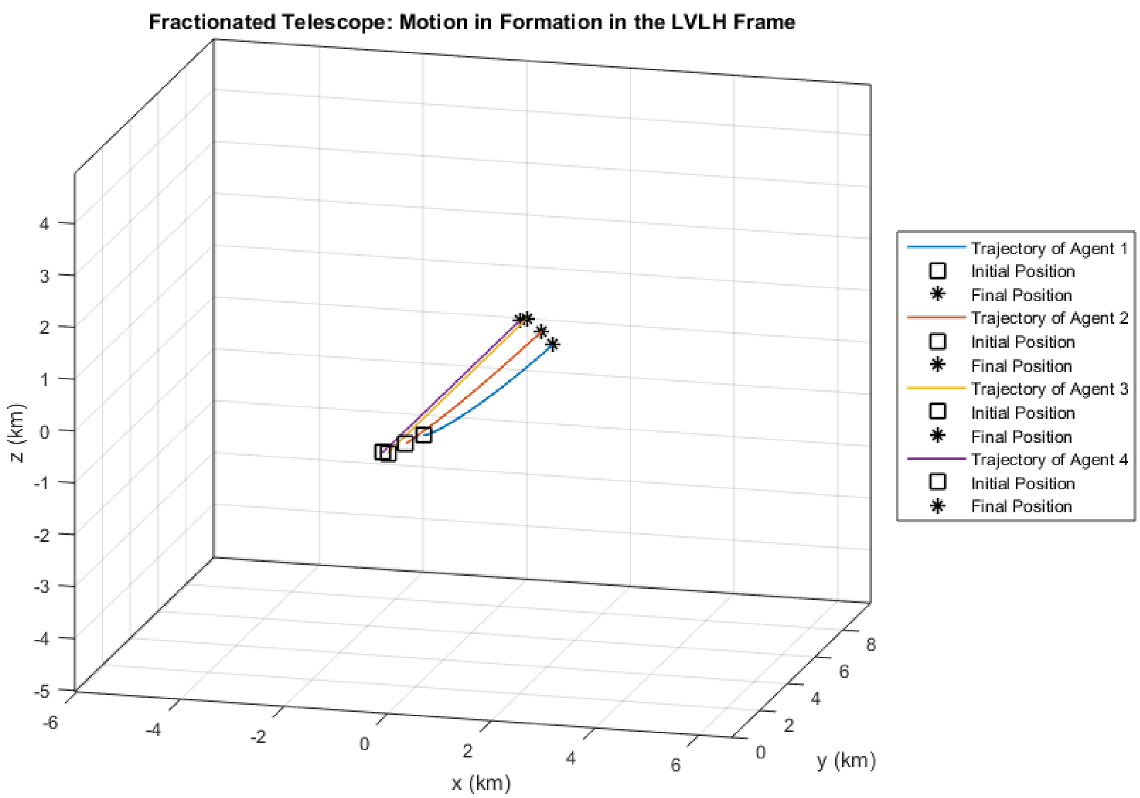

Figure 5.11. Motion of the Telescope Units in Formation

to the difference in length scale, the path of each agent is not clearly visible. Fig. (5.7) shows a zoomed-in view of the initial and final configurations of the telescope. The evolution of $(\delta x - h)$ over time has been plotted in Fig. (5.8).

Fig. (5.9) shows the control history for the nonlinear system. For comparison, the control history for the linearized system is shown in Fig. (5.9). These look very similar, because in comparison to the orbit radius, the length scale of the formation is very small. Moreover, the accelerations due to perturbations are very small (of the order of $10^{-9}\,\mathrm{km/s^2}$), because of which the linearized system represents the actual nonlinear system very well. For the next two examples, only the plots for the nonlinear system have been shown.

If the leader has an initial velocity of 0.01 km/s in the LVLH y-direction, the telescope moves in formation as shown in Fig. (5.11).

5.3 Reconfigurable Space Structures

Reconfigurable space structures (RSS) are fragmented structural components (scaffolds, trusses, booms, panels etc.) that may be used as parts of a very large spacecraft, such as a space station or observatory. These structural elements are themselves made of several smaller spacecraft, such as NanoSats or CubeSats. This concept, though relatively new, has gained traction in recent years. The use of RSS can make the the spacecraft an adaptive structure, which has numerous advantages.

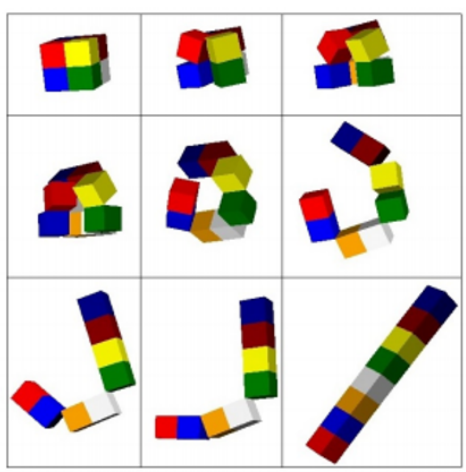

Figure 5.12. Reconfiguration of an RSS [21]

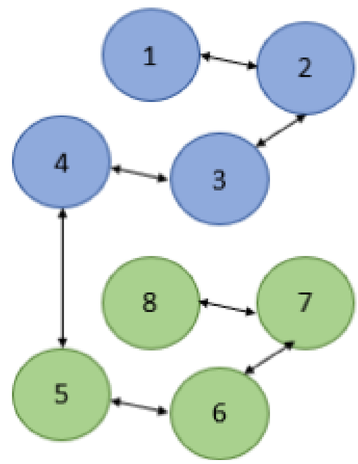

Figure 5.13. Communication Graph and Relative Initial Positions of the RSS (Not to Scale)

5.3.1 Motivation

Lattice-based RSS has been proposed by Ochalek et al. [22] for structural elements in space. Nisser [23] and a team at ESA [21] have proposed a concept for an RSS that is actuated electromagnetically. Taking this an inspiration, an alternative process is proposed for the reconfiguration, wherein the modules first separate (undock), then reconfigure in a free state, and finally dock to form a solid structure. The simulation for this example has been conducted for only the reconfiguration part, i.e., the simulation starts after the modules have undocked and ends when the target shape in the free state has been reached.

5.3.2 Problem Setup

One of the reconfigurations illustrated in [21] has been shown in Fig. (5.12), where the initial shape is a cube and the final shape is linear. The same reconfiguration has been simulated here. A potential application of such reconfiguration may be a modular robotic arm, which is folded into a cube for launch or storage purposes and extends to a linear configuration when deployed.

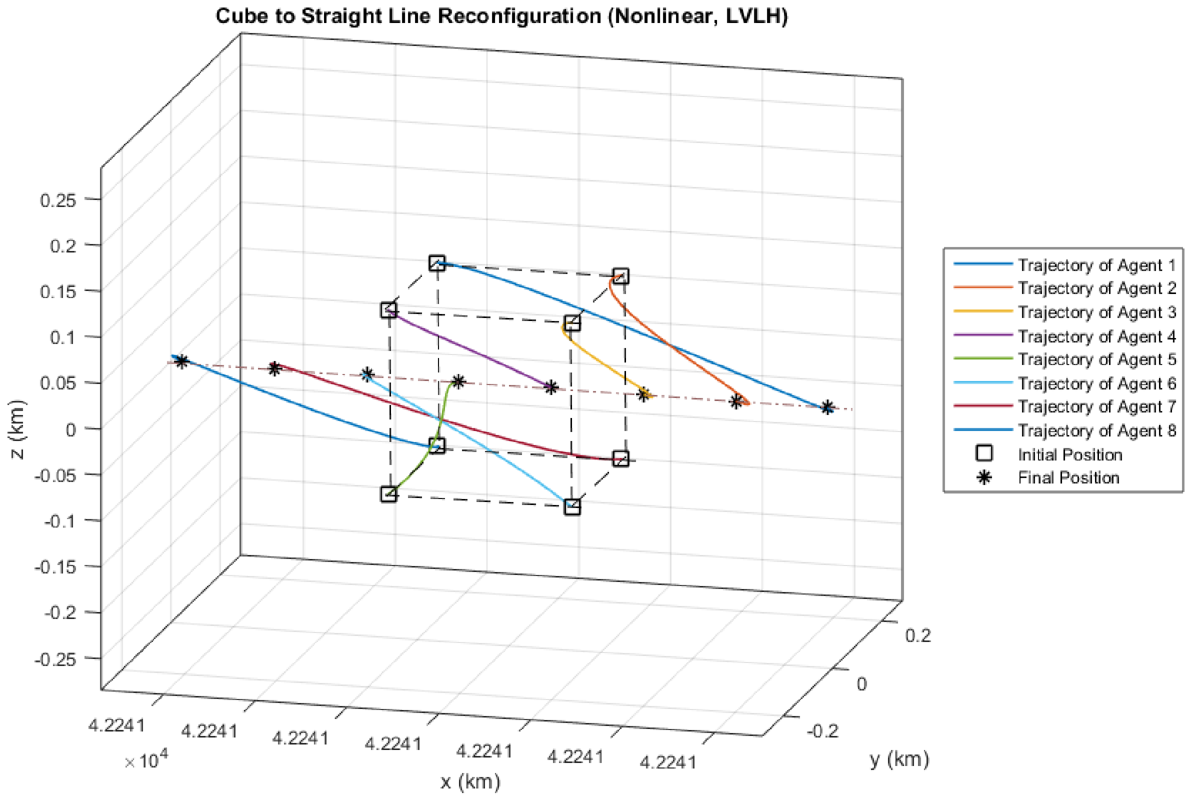

Figure 5.14. RSS Reconfiguration, LVLH Frame

For this simulation, the number of agents, $n = 8$. The initial configuration is a cube. The communication is bidirectional between adjacent neighbors. The communication graph and the relative positioning of the agents in the cubic form have been shown in Fig.(5.13). The final configuration is a straight line along the LVLH x-axis, which means that in the inertial frame, it is oriented radially outward form the central body. The inter-module separation distance in the initial and final configuration have been set as 200 m and 100 m respectively. The equilibrium point is the center of the initial cubic configuration, through which the geostationary reference orbit passes. Each agent in the formation is considered to be a 1U CubeSat (10 cm $\times$ 10 cm $\times$ 10 cm) with a mass of 2 kg. Both SRP and J_2 perturbations have been considered in this model.

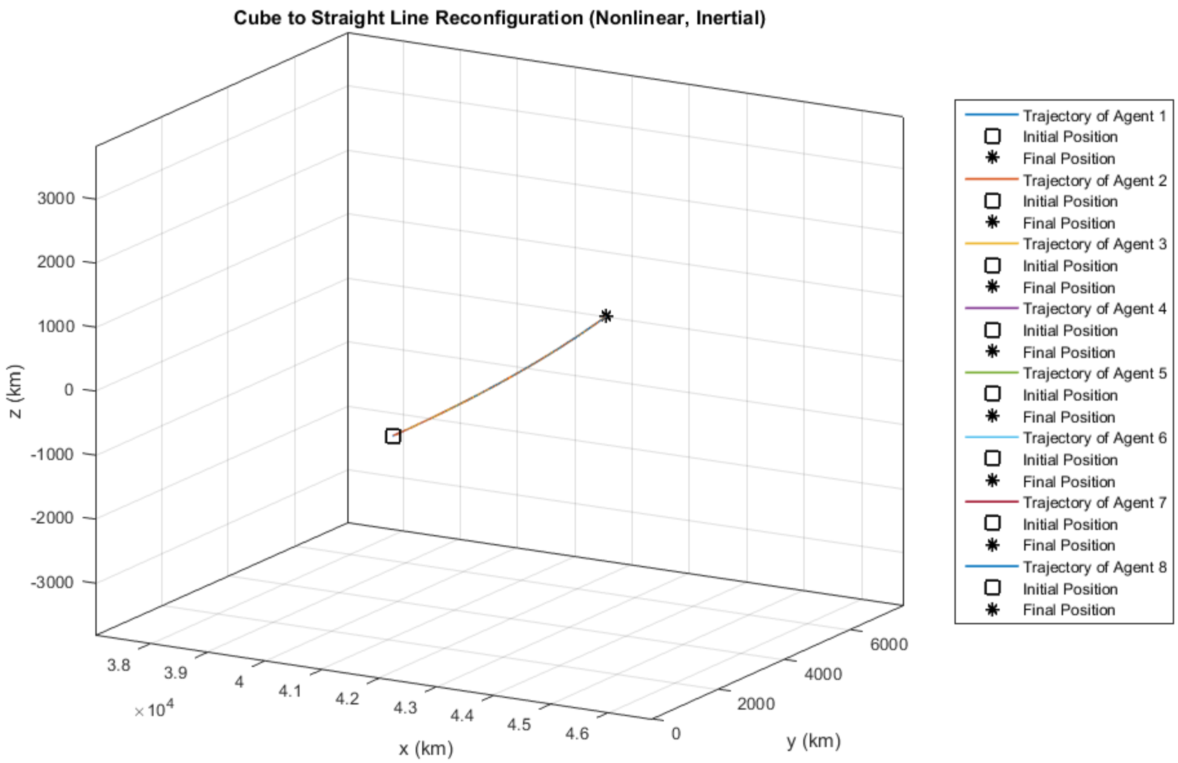

Figure 5.15. RSS Reconfiguration, Inertial Frame

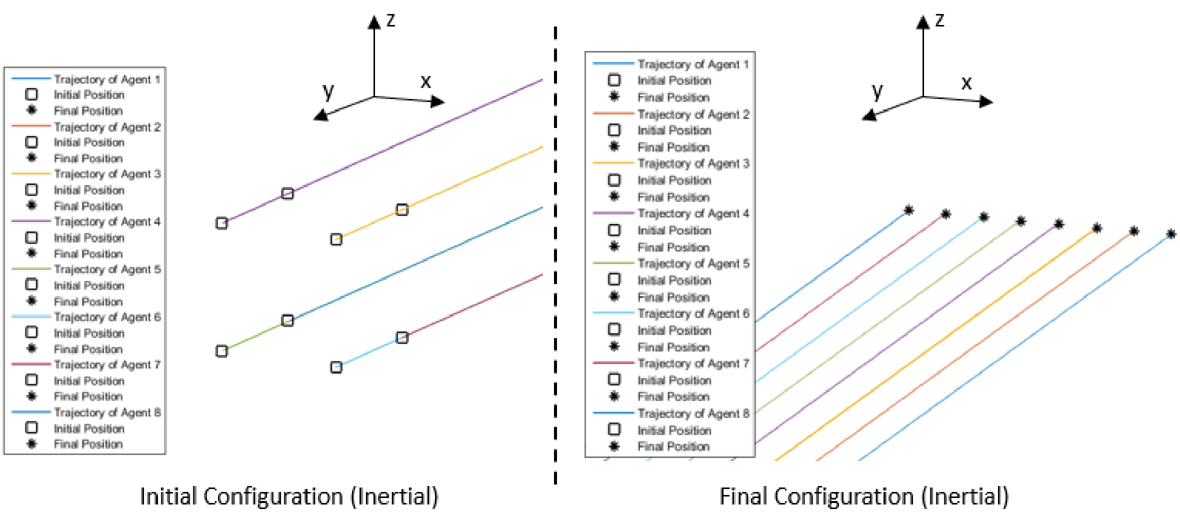

Figure 5.16. Initial and Final Configurations of the RSS, Inertial Frame

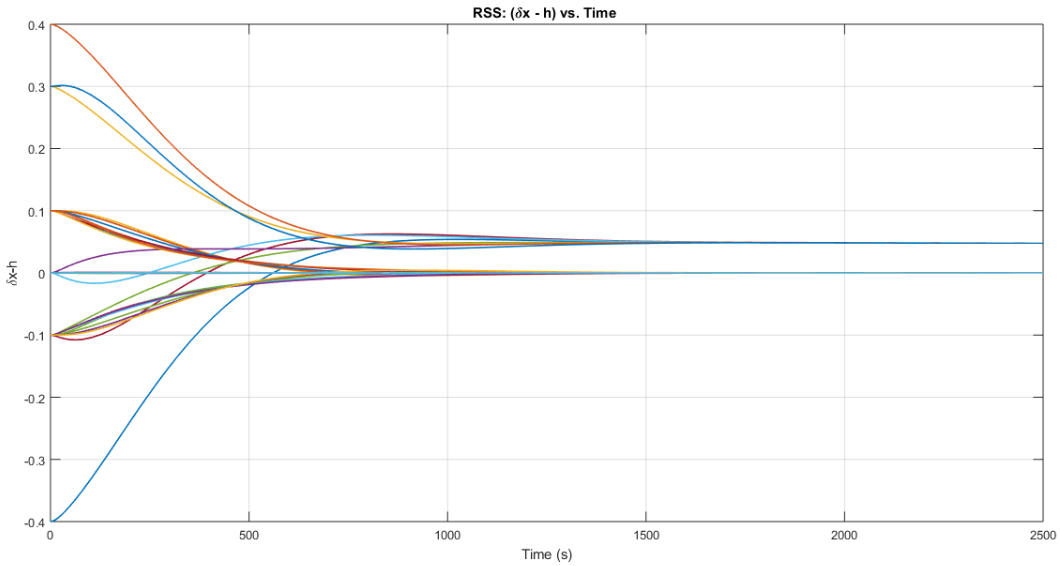

Figure 5.17. Evolution of $(\delta x - h)$ over Time for RSS Reconfiguration

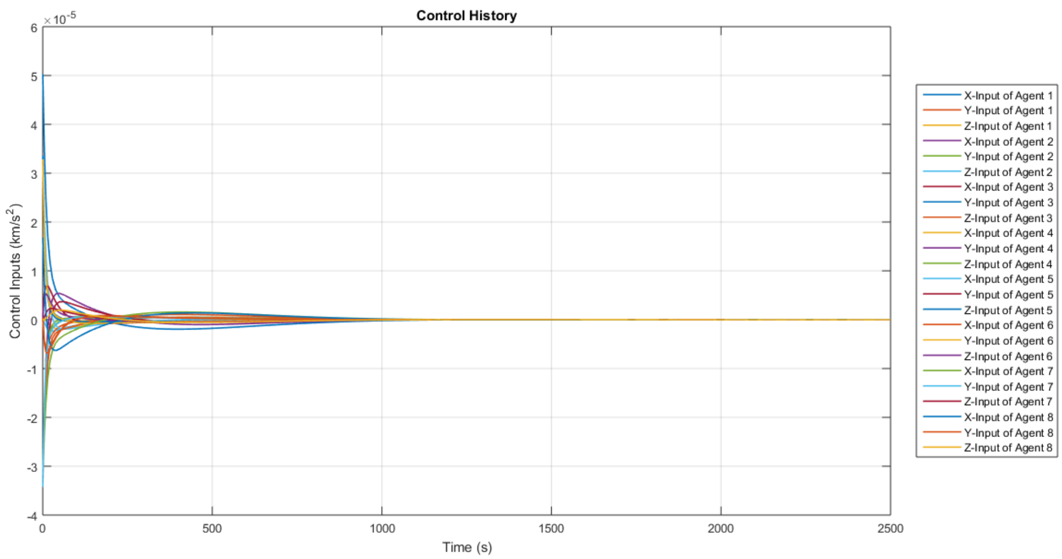

Figure 5.18. Control History of the RSS Reconfiguration

5.3.3 Simulation Results

The trajectory of the agents in the LVLH frame and the Inertial frame have been shown in Fig. (5.14) and Fig. (5.15) respectively. As the separation difference is small, the trajectory of the each agent is not distinguishable in the inertial frame. The zoomed-in plot in Fig.

(5.16) shows the initial and final configurations in the inertial frame. The plot of $(\delta x - h)$ as a function of time is shown in Fig. (5.17). It is observed that the some of the components of $(\delta x - h)$ converge to a nonzero value, i.e., the value of the offset p is not zero. The perturbations in this case can give rise to accelerations up to the order of 10^{-8} km/s^2. The control history is shown in Fig. (5.18).

5.4 Imaging and Interferometry

Formation-based Interferometry has been a long-researched topic. The concept was extensively studied for NASA's Terrestrial Planet Finder (2002 - 2011) [24] and ESA's Darwin (1993 - 2007) [25] projects, both of which were eventually cancelled. Despite this, the topic still evokes interest and there have been several new proposals for similar projects, like the StarLight mission, TandemX etc. Some aspects of this concept have also been tested in orbit.

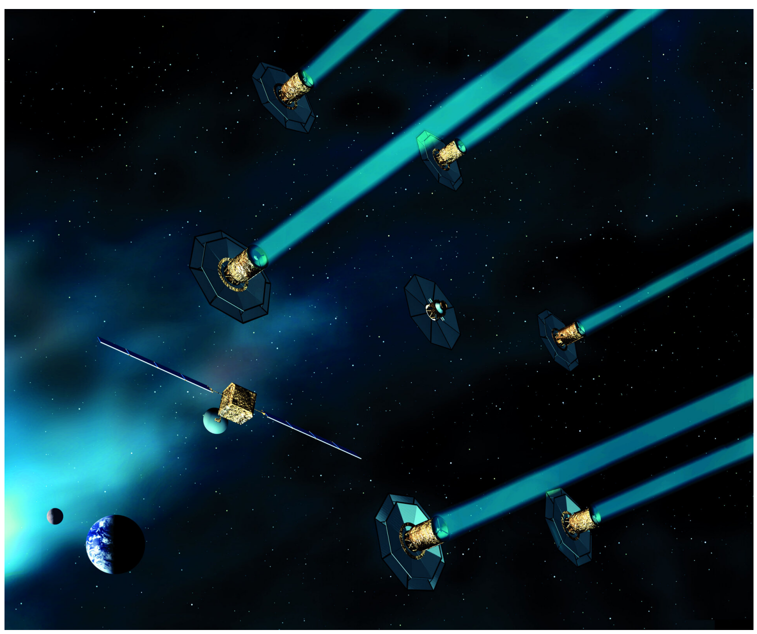

Figure 5.19. Artist's Impression of ESA Darwin [25]

Space-based interferometry ideally requires collectors distributed over a large area. This is difficult to do in a monolithic spacecraft, since it will increase its mass, size, and cost.

Therefore, a distributed system is preferred, where the collectors and optics units are divided among multiple spacecraft agents flying in formation.

5.4.1 Motivation

ESA's Darwin project, with the goal of searching for Earth-like planets, was proposed to have six peripheral collectors along with a central combiner and communication module. An artistic rendition of this concept is shown in Fig. (5.19). The StarLight mission [26] and others of its kind were inspired by this concept. For the simulation that follows, the number of peripheral agents have been expanded to 15 and the system goes from a linear rest configuration to a circular configuration when activated.

5.4.2 Problem Setup

The number of agents, $n = 16$. The communication architecture is of a leader-follower type, with the combiner as the leader. This was chosen since all the peripheral collectors must lie on a circle centered at the collector, which receives, processes and transmits their readings. The graph is represented in Fig. (5.20). The initial configuration is a line on the LVLH y-z plane, with a separation of 50 m between adjacent agents. The final configuration is a circle of radius 400 m, parallel to the y-z plane. The mass of each agent is taken as 100 kg and the area as 1 m^2. The equilibrium point coincides with the central combiner, which lies on a geostationary orbit at the initial time.

Apart from imaging and interferometry, this type of reconfiguration can potentially be used to change the inertia properties of adaptive space structures.

5.4.3 Simulation Results

The motion of the agents during the reconfiguration process has been represented in LVLH coordinates in Fig. (5.21). Fig. (5.22) shows the motion in the inertial frame. Due to small separation distances, the trajectories of all the agents appear as single curve in the inertial frame. The zoomed-in plot in Fig. (5.23) shows the initial and final configuration in the inertial frame. The acceleration due to perturbations in this simulation are of the order

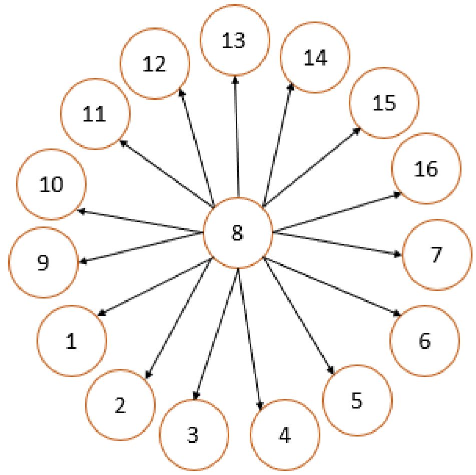

Figure 5.20. Interferometry Communication Graph

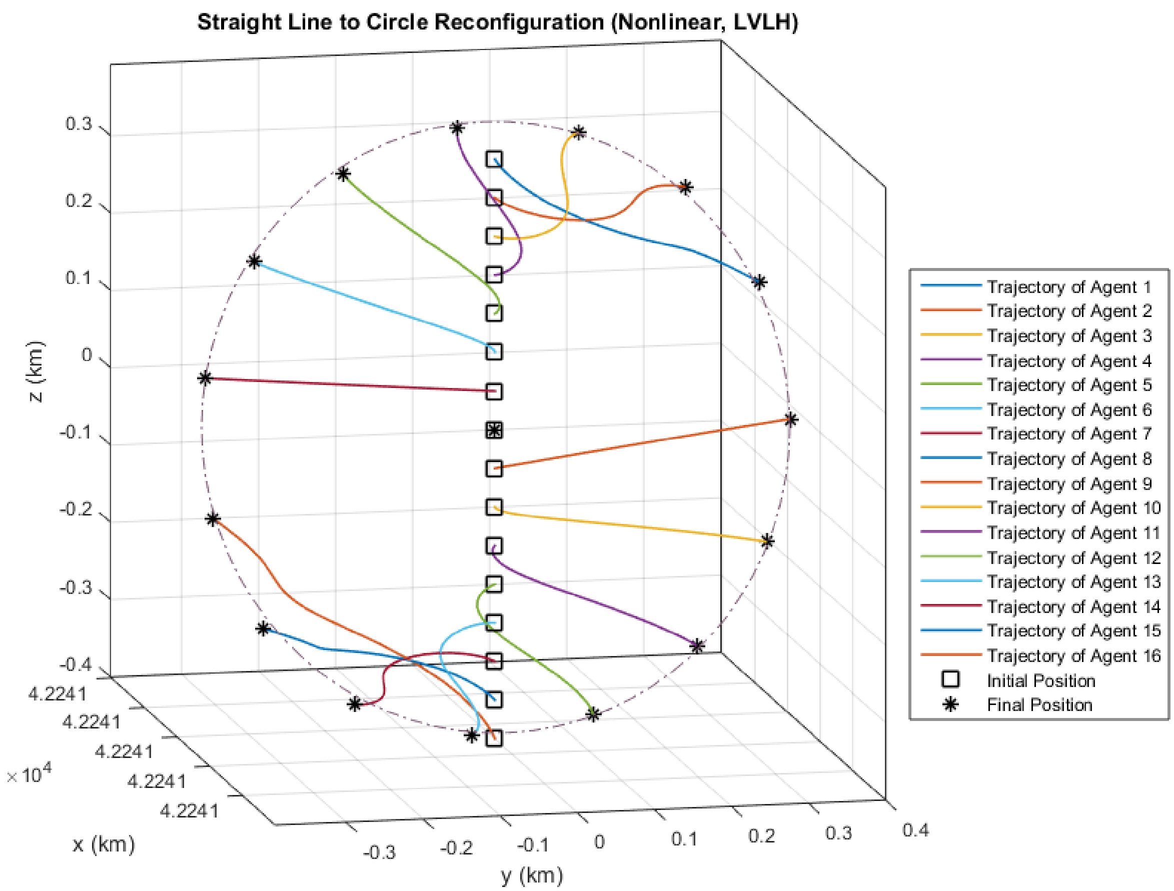

Figure 5.21. Interferometer Reconfiguration, LVLH Frame

of 10^{-9} km/s^2 . The time history of $(\delta x - h)$ has been plotted in Fig. (5.24). The control history is shown in Fig. (5.25).

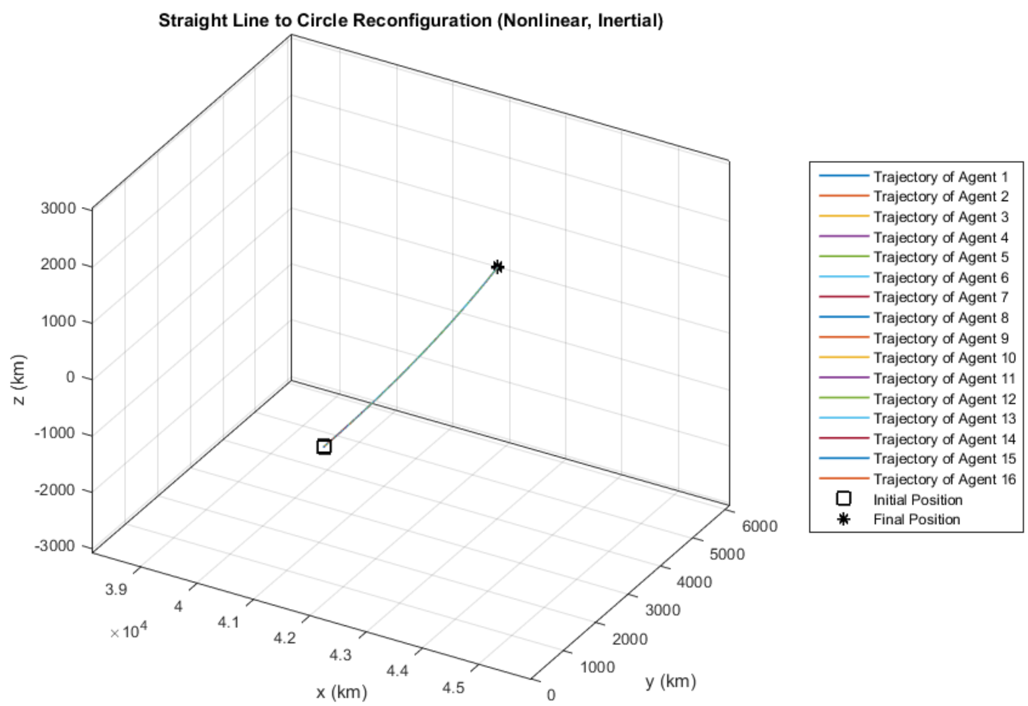

Figure 5.22. Interferometer Reconfiguration, Inertial Frame

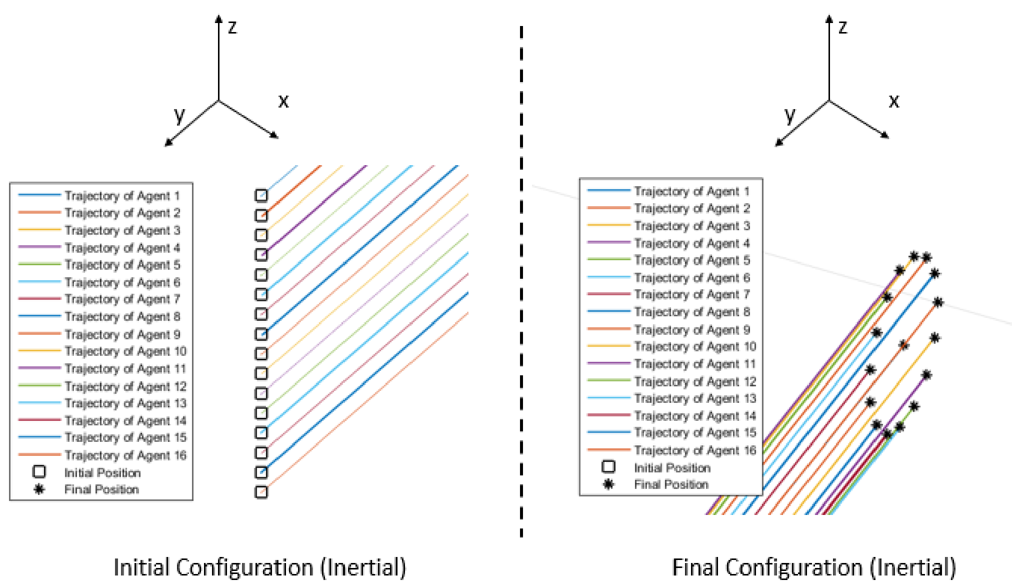

Figure 5.23. Initial and Final Configurations of the Interferometer, Inertial Frame

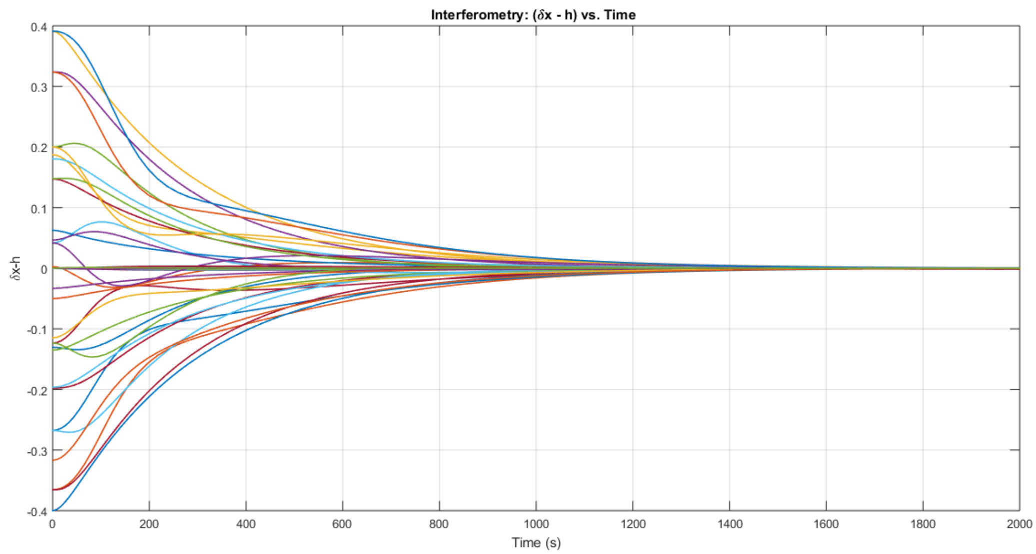

Figure 5.24. Evolution of $(\delta x - h)$ over Time for Interferometer Reconfiguration

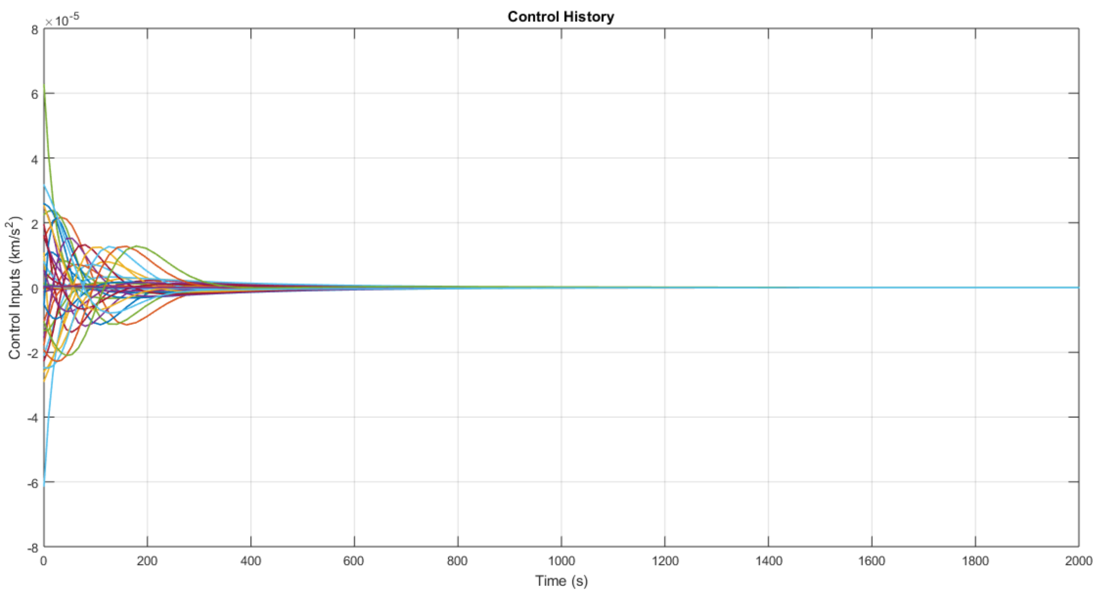

Figure 5.25. Control History of the Interferometer Reconfiguration

6. CONCLUSIONS

This thesis was motivated by the vast potential of adaptive spacecraft structures and formations and their scope of application in the future of space exploration, Earth observation, defense, telecommunication etc. In this thesis, the nonlinear dynamics were first linearized to derive a simple, manageable model. Two methods for driving a spacecraft formation to a new shape or configuration were discussed, both using this linearized model.

The first method discussed is the open-loop two point boundary value formulation. The initial configuration of the formation and the targeted state were used as the boundary conditions. A cost function was defined in order to minimize fuel consumption of the system. The Hamiltonian was derived and the Euler-Lagrange equations were solved to obtain a control profile that theoretically drives the spacecraft to its target configuration. However, in the practical world, this method is unlikely to be ideal.

Therefore, the derivation of a closed-loop control law was attempted. Information sharing was incorporated in the model. The agents of the formation were considered to be homogeneous from a control perspective for this problem.

6.1 Contribution of this Work

The contribution of this thesis is the derivation of a distributed closed-loop control law for the shape reconfiguration of a set of spacecraft agents flying in formation, whose dynamics are approximated by the Clohessy-Wiltshire system. Under this law, each agent utilizes its own information, as well as data received from its neighbors, to determine its trajectory. The multi-agent system is reformulated as a single-agent MIMO system. However, the distributed nature of the system is preserved by properly defining the concatenated system and its dynamics. The feedback gain matrix is dependent on the communication architecture of the formation. An explicit expression to select a stabilizing control gain matrix has been presented in this thesis. A range of gain matrices can be computed based on the dynamical equations (i.e., system and control matrices) and the eigenvalues of the graph Laplacian.

To validate the model, several applications have been demonstrated through simulations. These examples have been selected from various types of applications, namely, fractionated spacecraft, reconfigurable rigid structures, and free flying formations.

Some advantages of this formulation are listed here.

1. The control law translates well to the nonlinear system.
2. The method is scalable, as addition of more nodes does not significantly increase the complexity.
3. This formulation can be easily applied to any two-body system, by simply changing the μ value.
4. Being a feedback control system, it is capable of withstanding minor perturbing forces.
5. Exact final configuration need not be known; it is sufficient to specify only a target shape. The system converges to this shape while achieving velocity consensus.

Future scope of this work lies in the incorporation of collision avoidance capability in the model, improving the model of perturbing forces in the nonlinear system, and extension of the work to a wider range of applications.

REFERENCES

[1] K. Alfriend, S. R. Vadali, P. Gurfil, J. How, and L. Breger, *Spacecraft formation flying: Dynamics, control and navigation*. Elsevier, 2009, vol. 2.

[2] R. J. Glumb, C. Lietzke, S. Luce, and P. Wloszek, "Cubesat fourier transform spectrometer (cubesat-fts) for three-dimensional global wind measurements," 95th American Meteorological Society Annual Meeting, Phoenix, AZ, 2015.

[3] G. Sholomitsky, O. Prilulsky, and V. Rodin, "Infra-red space interferometer," 28th International Astronautical Congress, Prague, 1977.

[4] P. Wang and F. Hadaegh, "Coordination and control of multiple microspacecraft moving in formation," *Journal of the Astronautical Sciences*, vol. 44, no. 3, pp. 315–355, 1996. [Online]. Available: https://www.researchgate.net/publication/239062527_Coordination_and_control_of_multiple_microspacecraft_moving_in_formation.

[5] D. P. Scharf, F. Y. Hadaegh, and S. R. Ploen, "A survey of spacecraft formation flying guidance and control (Part II): Control," 2004 American Control Conference, Boston, MA, 2004.

[6] H. Schaub and K. T. Alfriend, "Hybrid cartesian and orbit element feedback law for formation flying spacecraft," *Journal of guidance, control, and dynamics*, vol. 25, no. 2, pp. 387–393, 2002.

[7] M. Mesbahi and F. Y. Hadaegh, "Formation flying control of multiple spacecraft via graphs, matrix inequalities, and switching," in *Proceedings of the 1999 IEEE International Conference on Control Applications (Cat. No. 99CH36328)*, IEEE, vol. 2, 1999, pp. 1211–1216.

[8] P. Wang and F. Y. Hadaegh, "Coordination and control of multiple microspacecraft moving in formation," 1996.

[9] R. Schlanbusch and P. J. Nicklasson, "Synchronization of target tracking cascaded leader-follower spacecraft formation," in *Advances in Spacecraft Technologies*, IntechOpen, 2011.

[10] P. Gurfil and D. Mishne, "Cyclic spacecraft formations: Relative motion control using line-of-sight measurements only," *Journal of guidance, control, and dynamics*, vol. 30, no. 1, pp. 214–226, 2007.

[11] C. R. McInnes, "Distributed control of maneuvering vehicles for on-orbit assembly," *Journal of Guidance, Control, and Dynamics*, vol. 18, no. 5, pp. 1204–1206, 1995.

[12] S. Bandyopadhyay, R. Foust, G. P. Subramanian, S.-J. Chung, and F. Y. Hadaegh, "Review of formation flying and constellation missions using nanosatellites," *Journal of Spacecraft and Rockets*, vol. 53, no. 3, 2016. DOI: 10.2514/8.8704. [Online]. Available: https://doi.org/10.2514/1.A33291.

[13] Wikipedia, *Integrated truss structure*, Nov. 2020. [Online]. Available: https://en.wikipedia.org/wiki/Integrated_Truss_Structure.

[14] H. Lim, H. Bang, and S. Lee, "Adaptive backstepping control for satellite formation flying with mass uncertainty," *Journal of Astronomy and Space Sciences*, vol. 23, no. 4, p. 405, 2006.

[15] W. H. Clohessy and R. S. Wiltshire, "Terminal guidance system for satellite rendezvous," *Journal of the Aerospace Sciences*, vol. 27, no. 9, pp. 653–658, 1960. DOI: 10.2514/8.8704. [Online]. Available: https://doi.org/10.2514/8.8704.

[16] G. Lafferriere, A. Williams, J. Caughman, and J. Veerman, "Decentralized control of vehicle formations," *Systems & control letters*, vol. 54, no. 9, pp. 899–910, 2005.

[17] W. Ren, R. W. Beard, and T. W. McLain, "Coordination variables and consensus building in multiple vehicle systems," in *Cooperative control*, Springer, 2005, pp. 171–188.

[18] AISolutions, *Solar radiation pressure*, 2015. [Online]. Available: https://ai-solutions.com/_help_Files/solar_radiation_pressure.htm.

[19] C. Xu, R. Tsoi, and N. Sneeuw, "Analysis of j2-perturbed relative orbits for satellite formation flying," in *Gravity, Geoid and Space Missions*, Springer, 2005, pp. 30–35.

[20] N. N. Lee, J. W. Burdick, P. Backes, S. Pellegrino, K. Hogstrom, C. Fuller, B. Kennedy, J. Kim, R. Mukherjee, C. Seubert, *et al.*, "Architecture for in-space robotic assembly of a modular space telescope," *Journal of Astronomical Telescopes, Instruments, and Systems*, vol. 2, no. 4, p. 041 207, 2016.

[21] M. Nisser, D. Izzo, and A. Borggraefe, "An electromagnetically actuated, self-reconfigurable space structure," *JSASS Aerospace Tech. Japan*, vol. 14, pp. 1–9, 2017.

[22] M. Ochalek, B. Jenett, O. Formoso, C. Gregg, G. Trinh, and K. Cheung, "Geometry systems for lattice-based reconfigurable space structures," in *2019 IEEE Aerospace Conference*, IEEE, 2019, pp. 1–10.

[23] M. Nisser, "Reconfigurable space structures," *Prototyping our Sci-Fi Space Future: Zero Gravity Flight Class (MAS.S66)*, 2020, https://zero-gravity.pubpub.org/pub/ghi03rl2. [Online]. Available: https://zero-gravity.pubpub.org/pub/ghi03rl2.

[24] NASA, *Terrestrial planet finder*, 2015. [Online]. Available: https://science.nasa.gov/missions/tpf.

[25] E. Medialab, *Darwin's six telescopes*, 2003. [Online]. Available: https://www.esa.int/ESA_Multimedia/Images/2015/06/Darwin_s_six_telescopes.

[26] G. H. Blackwood, O. P. Lay, W. D. Deininger, M. A. Gudim, A. Ahmed, R. M. Duren, C. Noecker, and B. Barden, "Starlight mission: A formation-flying stellar interferometer," in *Interferometry in Space*, International Society for Optics and Photonics, vol. 4852, 2003, pp. 463–480.

A. SAMPLE CODES

Sample Codes for the TPBVP Section

```
%% TPBVP Code %%

clc
clear

global w n A B Af Bf x0 xf

w=2*pi/(24*3600);    % Angular Velocity
mu=398600.4418;      % Gravitational Parameter of Central Body
x_e=(mu/w^2)^(1/3); % Equilibrium radial distance for circular orbit
d_s=0.0005*x_e;      % Separation distance, 0.05% of orbit radius

n = 3;


A=[ 0,        0,        0,        1,        0,        0;
    0,        0,        0,        0,        1,        0;
    0,        0,        0,        0,        0,        1;
    3*(w^2),0,        0,        0,        2*w,      0;
    0,        0,        0,        -2*w,     0,        0;
    0,        0,        -w^2,     0,        0,        0];

B=[ 0,0,0;
    0,0,0;
    0,0,0;
    1,0,0;
```

```
        0,1,0;
        0,0,1];

Af=kron(eye(n),A);
Bf=kron(eye(n),B);

x0=[0;0;0;0;0;0;
        0;d_s;0;0;0;0;
        0;2*d_s;0;0;0;0];

lambda0=(1e-5)*ones(size(x0));

xf=[0;0;0;0;0;0;
       -d_s*cosd(60);d_s*sind(60);0;0;0;0;
        d_s*cosd(60);d_s*sind(60);0;0;0;0];

tf=1800;

IG=[x0', lambda0'];

solinit = bvpinit(linspace(0,tf,10000), IG);
options = bvpset('Stats', 'on', 'RelTol', 1e-6);
sol = bvp4c(@BVP_ode, @BVP_bc, solinit, options);
t = sol.x;
y = sol.y;
% y = [x', lambda']'

states=y(1:6*n,:);
costates=y(6*n+1:12*n,:);
u=-Bf'*costates;
```

```
for k=1:length(t)

    U_max=3e-5;
    for j=1:3*n
        if u(j,k)<-U_max
            u(j,k)=-U_max;
        elseif u(j,k)>U_max
            u(j,k)=U_max;
        end
    end

    mag_u1(k)=norm(u(1:3,k));
    mag_u2(k)=norm(u(4:6,k));
    mag_u3(k)=norm(u(7:9,k));
    uTu(k)=u(:,k)'*u(:,k);
end

J=0.5*trapz(t,uTu);

for i=0:n-1
    rx(i+1,:)=states(6*i+1,:);
    ry(i+1,:)=states(6*i+2,:);
end

plotBVP(rx,ry)

plotBVPu(t,u)

%% Functions %%
```

```
function dydt = BVP_ode(t,y)

global n Af Bf

x = y(1:6*n);
lambda = y(6*n+1:12*n);
u = -Bf'*lambda;

U_max=3e-5;

for i=1:length(u)
    if u(i)<-U_max
        u(i)=-U_max;
    elseif u(i)>U_max
        u(i)=U_max;
    end
end

dydt = [Af*x + Bf*u;
        -Af'*lambda];

end



function res = BVP_bc(initial_conf,final_conf)

global n x0 xf

```

```
res = [initial_conf(1:6*n)-x0;
       final_conf(1:6*n)-xf];

end
```

Sample Codes for the Closed-Loop Section (Application: RSS)

Linearized System: Setup and Simulation

```
clear
clc

w=2*pi/(24*3600);     % Angular Velocity
mu=398600.4418;       % Gravitational Parameter of Central Body
x_e=(mu/w^2)^(1/3); % Equilibrium radial distance for circular
    orbit
Xe=[x_e;0;0;0;0;0]; % Equilibrium state for reference point

n=8;                  % Number of agents
O=ones(n,1);
Xef=kron(O,Xe);       % Concatenated reference state for formation

% Graph Laplacian %
% 1 <--> 2 <--> ... <--> 7 <--> 8 %
L=[1, -1, 0, 0, 0, 0, 0, 0;
   -1, 2, -1, 0, 0, 0, 0, 0;
   0, -1, 2, -1, 0, 0, 0, 0;
   0, 0, -1, 2, -1, 0, 0, 0;
   0, 0, 0, -1, 2, -1, 0, 0;
   0, 0, 0, 0, -1, 2, -1, 0;
   0, 0, 0, 0, 0, -1, 2, -1;
   0, 0, 0, 0, 0, 0, -1, 1];

% A and B for single spacecraft from CW Equations %
A=[ 0,      0,      0,      1,      0,      0;
    0,      0,      0,      0,      1,      0;
```

```
        0,          0,          0,          0,          0,          1;
        3*(w^2),0,          0,          0,          2*w,        0;
        0,          0,          0,          -2*w,       0,          0;
        0,          0,          -w^2,       0,          0,          0];

A_new=[ 0,          0,          0,          1,          0,          0;
        0,          0,          0,          0,          1,          0;
        0,          0,          0,          0,          0,          1;
        0,          0,          0,          0,          2*w,        0;
        0,          0,          0,          -2*w,       0,          0;
        0,          0,          0,          0,          0,          0];

B=[ 0,0,0;
    0,0,0;
    0,0,0;
    1,0,0;
    0,1,0;
    0,0,1];

W=[3*(w^2), 0,          0,          0,          2*w,        0;
        0,          0,          0,          -2*w,       0,          0;
        0,          0,          -w^2,       0,          0,          0];

% LQR Definition %
q=5e-10;
Q=q*eye(6);
R=eye(3);
K_int=-lqr(A,B,Q,R);
gamma=7.5;
K=gamma*K_int;
```

```
% Concatenated Matrices for the formation %
Af=kron(eye(n),A);
Bf=kron(eye(n),B);
Lf=kron(L,eye(6));
Kf=kron(eye(n),K);
Wf=kron(eye(n),W);

% Change of states from delta x to (delta x - h) %
Bff=[Bf, eye(6*n)];
Df=zeros(size(Bff));

% Initial and Target States (Linearized)%
deltax0=[-0.1;  0.1;    0.1;    0;  0;  0;
          0.1;  0.1;    0.1;    0;  0;  0;
          0.1; -0.1;    0.1;    0;  0;  0;
         -0.1; -0.1;    0.1;    0;  0;  0;
         -0.1; -0.1;   -0.1;    0;  0;  0;
          0.1; -0.1;   -0.1;    0;  0;  0;
          0.1;  0.1;   -0.1;    0;  0;  0;
         -0.1;  0.1;   -0.1;    0;  0;  0];

h=[ 0.3;    0;  0;  0;  0;  0;
    0.2;    0;  0;  0;  0;  0;
    0.1;    0;  0;  0;  0;  0;
    0.0;    0;  0;  0;  0;  0;
   -0.1;    0;  0;  0;  0;  0;
   -0.2;    0;  0;  0;  0;  0;
   -0.3;    0;  0;  0;  0;  0;
   -0.4;    0;  0;  0;  0;  0];
```

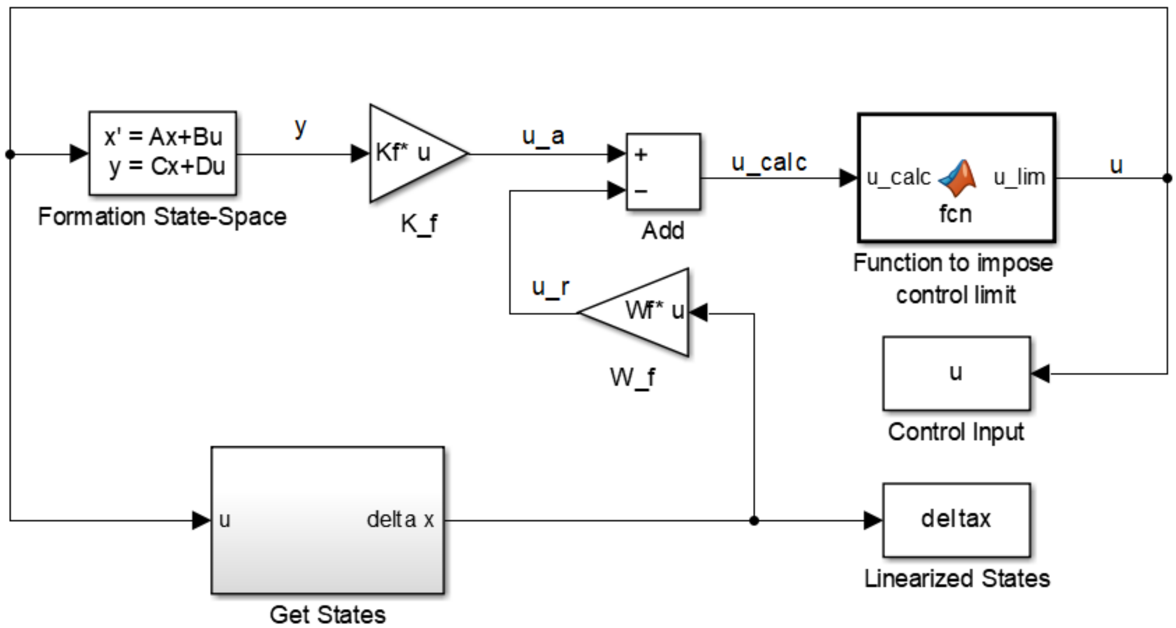

Figure A.1. Simulink® Model for Linearized System

Nonlinear System: Integration and Simulation

```
function [sys,x0,str,ts] = SFunction_NL(t,x,u,flag)

% t is time
% x is state
% u is input
% flag is a calling argument used by Simulink.
% The value of flag determines what Simulink wants to be executed.

global n mu w

n=8;
w=2*pi/(24*3600);
```

```
mu=398600.4418;

switch flag

case 0                              % Initialization
    [sys,x0,str,ts]=mdlInitializeSizes;

case 1                              % Compute Derivatives xdot
    sys=mdlDerivatives(t,x,u);

case 2                              % Not needed for continuous-time systems

case 3                              % Compute Output
    sys = mdlOutputs(t,x,u);

case 4                              % Not needed for continuous-time systems

case 9                              % Not needed here

end

%%%%%%%%%%%%%%%%%%%%%%%%%%%%%%%%%%%%%
% mdlInitializeSizes %
%%%%%%%%%%%%%%%%%%%%%%%%%%%%%%%%%%%%%
%
function [sys,x0,str,ts]=mdlInitializeSizes

global n mu w
```

```
% Create the sizes structure %
sizes=simsizes;
sizes.NumContStates = 6*n;          % Set number of continuous-time
    state variables
sizes.NumDiscStates = 0;
sizes.NumOutputs = 6*n;             % Set number of outputs
sizes.NumInputs = 3*n;              % Set number of intputs
sizes.DirFeedthrough = 0;
sizes.NumSampleTimes = 1;           % Need at least one sample time
sys = simsizes(sizes);

% Reference Point %
x_e=(mu/w^2)^(1/3);
Xe=[x_e;0;0;0;0;0];
O=ones(n,1);
Xef=kron(O,Xe);

% Initial states (linearized and nonlinear)
deltax0=[   -0.1;    0.1;    0.1;    0;   0;   0;
             0.1;    0.1;    0.1;    0;   0;   0;
             0.1;   -0.1;    0.1;    0;   0;   0;
            -0.1;   -0.1;    0.1;    0;   0;   0;
            -0.1;   -0.1;   -0.1;    0;   0;   0;
             0.1;   -0.1;   -0.1;    0;   0;   0;
             0.1;    0.1;   -0.1;    0;   0;   0;
            -0.1;    0.1;   -0.1;    0;   0;   0];
x0=Xef+deltax0;

str=[];                            % str is always an empty matrix
```

```
ts=[0 0];                        % ts must be a matrix of at least
    one row and two columns

%%%%%%%%%%%%%%%%%%%%%%%%%%%%%%%%%%%%%%%%

%%%%%%%%%%%%%%%%%%%%%%%%%%%%%%%%%%%%%%%%
% mdlDerivatives
%%%%%%%%%%%%%%%%%%%%%%%%%%%%%%%%%%%%%%%%
%
function sys = mdlDerivatives(t,x,u)

% Compute xdot based on (t,x,u) and set it equal to sys

global n mu w

% Set the Derivatives %

for i=1:n
    x_i=x(6*(i-1)+1);
    y_i=x(6*(i-1)+2);
    z_i=x(6*(i-1)+3);
    dx_i=x(6*(i-1)+4);
    dy_i=x(6*(i-1)+5);
    dz_i=x(6*(i-1)+6);

    ux_i=u(3*(i-1)+1);
    uy_i=u(3*(i-1)+2);
    uz_i=u(3*(i-1)+3);

    r=sqrt(x_i^2+y_i^2+z_i^2);
```

```
k=mu/r^3;

% Calculation for SRP Acceleration %
area=0.1*0.1;
m_sc=2;
a_SRP=0.4557*(10^(-8))*area/m_sc;

% Calculation for J2 Acceleration %
TM1=[cos(w*t),      -sin(w*t),     0;
     sin(w*t),       cos(w*t),     0;
     0,              0,        1];     % Transformation Matrix,
        LVLH to Inertial

TM2=[cos(w*t),       sin(w*t),     0;
    -sin(w*t),       cos(w*t),     0;
     0,              0,        1];     % Transformation Matrix,
        Inertial to LVLH

J2=1.0826*10^(-3);
C=1.5*mu*J2*(6378^2)/(r^5);

xyz_in=TM1*[x_i; y_i; z_i];
jx=C*xyz_in(1)*(5*(xyz_in(3)/r)^2-1);
jy=C*xyz_in(2)*(5*(xyz_in(3)/r)^2-1);
jz=C*xyz_in(3)*(5*(xyz_in(3)/r)^2-3);

J2_r=TM2*[jx; jy; jz];      % Conversion from Inertial to
    Rotating Frame
a_J2_x=J2_r(1);
a_J2_y=J2_r(2);
```

```
        a_J2_z=J2_r(3);

        % Derivatives %
        ddx_i=2*w*dy_i+(w^2-k)*x_i+ux_i+a_SRP*abs(cos(w*t/2))+a_J2_x;
        ddy_i=-2*w*dx_i+(w^2-k)*y_i+uy_i+a_SRP*abs(sin(w*t/2))+a_J2_y;
        ddz_i=-k*z_i+uz_i+a_J2_z;

        sys(6*(i-1)+1) = dx_i;
        sys(6*(i-1)+2) = dy_i;
        sys(6*(i-1)+3) = dz_i;
        sys(6*(i-1)+4) = ddx_i;
        sys(6*(i-1)+5) = ddy_i;
        sys(6*(i-1)+6) = ddz_i;
end

%%%%%%%%%%%%%%%%%%%%%%%%%%%%%%%%%%%%%%%%%%%%%%

%%%%%%%%%%%%%%%%%%%%%%%%%%%%%%%%%%%%%%%%%%%%%%
% mdlOutput
%%%%%%%%%%%%%%%%%%%%%%%%%%%%%%%%%%%%%%%%%%%%%%
%
function sys = mdlOutputs(t,x,u)

% Compute output based on (t,x,u) and set it equal to sys

global n

for i=1:n
        sys(6*(i-1)+1) = x(6*(i-1)+1);   %x_i
```

```
        sys(6*(i-1)+2) = x(6*(i-1)+2);   %y_i
        sys(6*(i-1)+3) = x(6*(i-1)+3);   %z_i
        sys(6*(i-1)+4) = x(6*(i-1)+4);   %dx_i
        sys(6*(i-1)+5) = x(6*(i-1)+5);   %dy_i
        sys(6*(i-1)+6) = x(6*(i-1)+6);   %dz_i
end
```

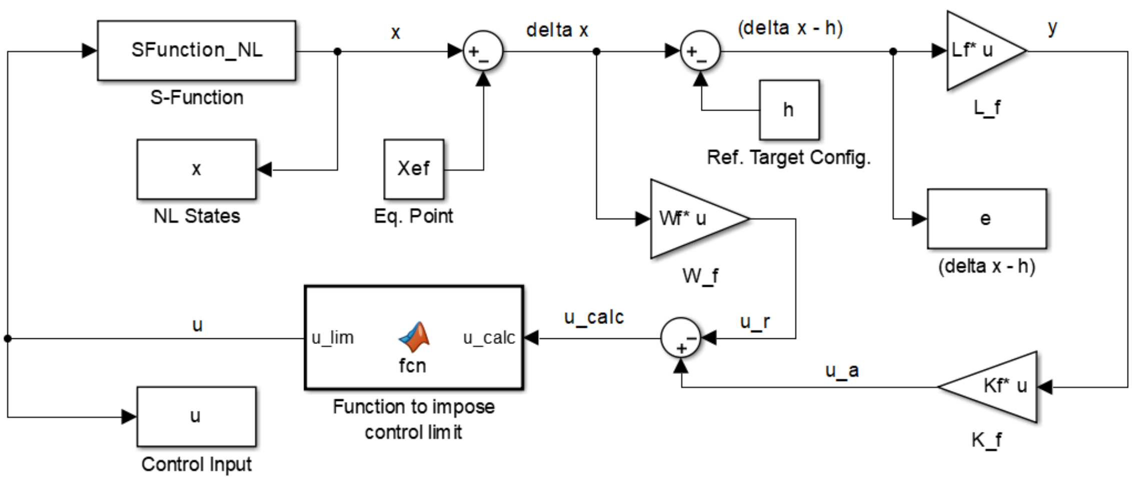

Figure A.2. Simulink® Model for Nonlinear System